A COMPREHENSIVE FEM MODELING OF 3-PHASE INDUCTION MOTOR WITH STATOR INTER-TURN FAULT

A Thesis Submitted in the partial fulfilment of the requirements for the degree of

MASTER OF ELECTRICAL ENGINEERING (MACHINE)

Submitted by

MEGHNAD HEMBRAM

Examination Roll Number: **M4ELE19017**

Registration Number: **111739** of **2010–2011**

Under the Guidance of

Prof. Madhab Roy,

Prof. Arabinda Das
and
Prof. Susanta Ray

Electrical Engineering Department

Faculty Council of Engineering and Technology

JADAVPUR UNIVERSITY

KOLKATA–700032

MAY, 2019

Faculty Council of Engineering and Technology

JADAVPUR UNIVERSITY

KOLKATA- 700032

Certificate of Recommendation

This is to certify that Mr. Meghnad Hembram (Examination Roll No. M4ELE19017) has completed his dissertation entitled, **"A Comprehensive FEM Modeling of 3-Phase Induction Motor with Stator Inter-turn Fault"**, under the direct supervision and guidance of Prof. Madhab Roy, Associate Professor, Electrical Engineering Department, Jadavpur University and, Prof. Arabinda Das, Professor, Electrical Engineering Department, Jadavpur University and, Prof. Susanta Ray, Assistant Professor, Electrical Engineering Department, Jadavpur University. We are satisfied with his work, which is being presented for the partial fulfillment of the degree of Master of Electrical Engineering (Machine) of Jadavpur University, Kolkata-700032.

Arabinda Das

Prof. Madhab Roy	*Prof. Arabinda Das*	*Prof. Susanta Ray*
Associate Professor	*Professor*	*Assistant Professor*
Department of Electrical Engineering	*Department of Electrical Engineering*	*Department of Electrical Engineering*
Jadavpur University, Kolkata – 700032	*Jadavpur University, Kolkata – 700032*	*Jadavpur University, Kolkata – 700032*

Prof. Kesab Bhattacharyya	*Prof. Chiranjib Bhattacharjee*
Head	*Dean*
Electrical Engineering Department	*Faculty Council of Engineering and Technology*
Jadavpur University, Kolkata – 700032	*Jadavpur University, Kolkata – 700032*

Faculty Council of Engineering and Technology

JADAVPUR UNIVERSITY

KOLKATA- 700032

*Certificate of Approval **

The forgoing thesis, entitled as **"A Comprehensive FEM Modeling of 3-Phase Induction Motor with Stator Inter-turn Fault"** is hereby approved by the committee of final examination for evaluation of thesis as a creditable study of an engineering subject carried out and presented by **Mr. Meghnad Hembram** (Examination Roll No.: M4ELE19017) , Registration No 111739 of 2010-11) in a manner satisfactory to warrant it's acceptance as a perquisite to the degree of **Master of Electrical Engineering (Machine).** It is understood that by this approval, the undersigned do not necessarily endorse or approve any statement made, opinion expressed or conclusion drawn therein, but approve the thesis only for the purpose for which it is submitted.

FINAL EXAMINATION FOR EVALUATION OF THE THESIS

_____

_____

_____

_____

Signature of Examiners

**Only in case thesis is approved*

Declaration of Originality and Compliance of Academic Ethics

I hereby declare that this thesis contains literature survey and original research work done by me. All the information in this document have been obtained and presented in accordance with academic rules and ethical conduct. I also declare that, as required by these rules and conduct, I have fully cited and referenced all material and results that are not original to this work.

Name (in Block Letters) **: MEGHNAD HEMBRAM**

Examination Roll No. **: M4ELE19017**

Thesis Title **: A Comprehensive FEM Modeling of 3-Phase Induction Motor with Stator Inter-turn Fault.**

Signature with Date **:**

ACKNOWLEDGEMENT

This report is the summary of my thesis works from June 2018 to May 2019 as a member of Simulation laboratory of Jadavpur University. I would like to express my acknowledgements to many people for their encouragements and supports.

First of all, I would like to express my sincere gratitude to my supervisors, Prof. Madhab Roy and Prof. Arabinda Das and Prof. Susanta Ray of Department of Electrical Engineer of Jadavpur University for their motivation, guidance and valuable suggestions. They helped me to develop my engineering skills as well as my other interpersonal skills.

I am also thankful to my friends for their motivation and all sorts of help.

I would like to thank AICTE for their financial support.

Last but not the least I want to place my gratitude to my parents and family members who have been constant source of inspiration in perusing my career.

Meghnad Hembram

Jadavpur University

Kolkata-700032

ABSTRACT

The dependency of major industries on Induction Motors cannot be understated. Production of these industries depends upon the reliable operation of these motors. Sudden failure of a machine may lead to huge economic loss. There are different sources of failure in an induction motor, among them bearing faults and stator inter turn fault are more common. Early detection of these faults is the only solution of preventing the machine as well as the process from devastating consequences. The stator-inter turn fault has been addressed in this research work which is based on an FEM model because among different types of approaches finite element methods(FEM) can imitate the physical machine more accurately. COMSOL Multiphysics has been chosen as the simulation tool. Simulation of the induction motor is performed with the help of this tool for two conditions. One is healthy condition and other is faulty condition. Here inter-turn fault in stator winding has only been considered. All the faults are taken as they are in their incipient stages. The stator current signature has taken for analysis. The results show that the slot harmonics have significant contribution in characterizing the stator winding inter-turn fault.

Table of Contents

Acknowledgement ..... **i**
Abstract ..... **ii**
List of Figures ..... **v**
List of Tables ..... **viii**
List of Acronyms ..... **ix**
List of Symbols ..... **x**
1. Chapter I **1**
Introduction: **1**
1.1 Motivation of the Work: **1**
1.2 Objectives: **2**
1.3 Literature Review: **3**
1.4 Outline of the Thesis: **4**
2. Chapter II **5**
Finite Element Method **5**
2.1 Background of Finite Element Method: **5**
2.2 The Finite Difference Method (FDM): **5**
2.3 The Finite Volume Method (FVM): **5**
2.4 The Boundary Element method (BEM): **6**
2.5 Finite Element Method (FEM): **6**
2.5.1 General: **6**
2.5.3 Computation process of FEM: **10**
2.6 Software introduction to implement the FEM: **21**
3. Chapter III **22**
Faults in Induction Motor: **22**
3.1 Induction Motor: **22**
3.2 Type of faults: **23**
3.3 Short circuit fault: **23**
3.4 Rotor bar and ring Fault: **24**
3.5 Bearing Fault: **24**

3.6 Air gap eccentricity fault: 25
4. Chapter IV 27
FEM Modeling of Squirrel Cage Induction Motor: 27
4.1 The work definition: 27
4.2 FEM Modeling: 32
4.3 Model specification: 33
4.4 Modeling of Geometry: 33
4.5 Assignment of Materials: 34
4.6 Assignment of physics or Equations: 34
4.7 FEM Mesh Generation: 41
5. Chapter V 45
Result and Discussion 45
5.1 introduction: 45
5.2 Validation of Model: 45
5.3 Results of Healthy and Faulty Conditions: 51
5.4 Method of Stator Current Analysis: 55
5.5 Observations: 58
6. Chapter VI 62
Conclusion and Future Work 62
6.1 Conclusions: 62
6.2 Scope of Future Work: 62
7. Chapter VII 63
Reference 63

List of Figures

2.1	Circle with elements	7
2.2	Arbitrary geometry with elements	9
2.3	Elements in 1D, 2D and 3D	9
2.4	(a)The solution region; (b) its finite element discretization	11
2.5	Typical triangular element; local node numbering 1-2-3 must proceed counter-clockwise as indicated by the arrow	13
2.6	The shape functionsα_1, α_2 and α_3 for triangular element	14
2.7	Discretization of an in homogeneous solution region	16
2.8	Assembly of three elements; i-j-k corresponds to local numbering (1-2-3) of the element in Fig. 2.5	17
2.9	A solution region that is symmetric along the y-axis	21
3.1	Possible failure Modes of Y-connected Stator	24
3.2	Typical structure of a rolling-element bearing with main parameters	25
4.1	stator slot dimensions	28
4.2	rotor slot dimensions	30
4.3	Geometry of squirrel cage IM in 2D	34
4.4	Definition of boundary condition	37
4.5	External stator electrical circuit for one phase	39
4.6	External rotor electrical circuit for one phase	40
4.7	Typical finite elements in the two dimensional x − y plane	42
4.8	Three phase induction motor is meshed by triangles	42
4.9	the enlarged region of the half of the three-phase motor	43

4.10	Air gap meshing	44
5.1	Three phaseCoil Voltage of stator	46
5.2	Torque vs time Characteristics	47
5.3	No load 3 phase current of stator	48
5.4	No load speed vs time characteristic	49
5.5	Motor 2D model with one phase coils	49
5.6	Magnetic Flux density norm	50
5.7	Current Density Norm	50
5.8	Stator Coil voltage for Healthy condition	51
5.9	Stator coil Current for Healthy condition	51
5.10	Stator coil voltages for faulty condition considering 2 turns short	52
5.11	Stator coil current for faulty condition considering 2 turns short	52
5.12	Stator coil voltage for faulty condition considering 4 turns short	52
5.13	Stator coil current for faulty condition considering 4 turns short	53
5.14	Stator coil voltage for faulty condition considering 6 turns short	53
5.15	Stator coil current for faulty condition considering 6 turns short	54
5.16	Stator coil voltage for faulty condition considering 8 turns short	54
5.17	Stator coil current for faulty condition considering 8 turns short	54
5.18	Stator coil voltage for faulty condition considering 116 turns short	55
5.19	Stator coil current for faulty condition considering 116 turns short	55
5.20	Overlapping of healthy faulty phase currents	58
5.21	2nd phase's current waveform	59
5.22	3rd phase's current waveform	59

5.23 current waveform of 2nd & 3rd phase considering phase shifting 60

5.24 frequency spectrum (Continuous FFT) of faulted phase currents 60

5.25 Comparison of Current density between healthy and 116 short turn condition 61

List of Tables

4.1	Some dimensions of SCIM	33
5.1	Validation of parameters	45

List of Acronyms

FEM	Finite Element Method
BEM	Boundary Element Method
FDM	Finite Differential Method
FVM	Finite Volume Method
IM	Induction Motor
SCIM	Squirrel Cage Induction Motor

List of Symbols

List of Symbols

V	: Volt
A	: Ampere
H	: Henry
mm	: Millimeter
m	: Meter
Wb	: Weber
$N-m$	: Newton-meter
$=$	: Equal to
$\approx$	: Approximately equal to
$\neq$	: Not equal to
X^{-1}	: Inverse of X
$\lvert X \rvert$	: Determinant of X

1. Chapter I

Introduction

1.1 Motivation of the Work:

Induction motors are becoming more popular in industries and in our everyday life for some specific advantages. [1] Induction motor is the most cost effective among all conventional machines therefore the usage of machine is shifting towards induction machine. Apart from cost it is mechanically robust, brush less, smooth speed control, simple & rugged in construction, high starting torque etc. Now if we consider induction motor there are many fault occurrences due to thermal, electrical, mechanical and environmental reasons. Early detection of fault may lead to overcome the costly machinery repair, down time and safety operations. [2] Among many of faults stator failure is more dominant which is approximately 36% of induction motor failure. Stator winding fault may occur as inter-turn short circuit, coil to coil, phase to phase and phase to ground. Early detection of these faults are more important to ignore severe damage of the induction motor.

There are no such reliable methods of detection of induction motor faults because of two main issues. [3] Firstly, the modeling of the induction motor under fault conditions, in the lack of comprehensive field fault database. Secondly the algorithm which address the difficulty in distinguishing between degree of faults.

In this century field computation method of modeling is developing rapidly as computer usage in real life. Finite element method of computation is becoming more popular as it's more convergent to solution. Here we tried to characterize the behavior of harmonics of stator current (Induction motor) with inter-turn fault condition. [4] We used COMSOL Multiphysics (which is FEM tool) to simulate this fault. We modeled induction motor in 2-D solid system with externally coupled circuit.

1.2 Objectives:

It is known that induction motors are becoming more popular in industries and in our everyday life for some specific advantages. Induction motor is the most cost effective among all conventional machines therefore the usage of machine is shifting towards induction machine. Apart from cost it is mechanically robust, brush less, smooth speed control, simple & rugged in construction, high starting torque etc. Now if we consider induction motor there are many fault occurrences due to thermal, electrical, mechanical and environmental reasons. Early detection of fault may lead to overcome the costly machinery repair, down time and safety operations. Among many of faults stator failure is more frequent which is approximately 36% of induction motor failure. Stator winding fault may occur as inter-turn short circuit, coil to coil, phase to phase and phase to ground. Early detection of these faults are more important to ignore severe damage of the induction motor. This fault can be analysed by many tools. But modeling of the fault condition is more difficult or complicated. That is more generalized to model these conditions if we modeled by FEM.

Here we focused on Finite Element Method of computation. The value of time dependent variable in different point of geometry can be solve by FEM. Usually Time dependent problems are expressed in terms of Partial Differential Equations (PDEs). There are many methods to solve PDEs but FEM is more conversed to solution then other method. Therefore, we have chosen a FEM base Tool (COMSOL Multiphysics) to simulate the induction motor for particular analysis. Although these tools are not developed so well to reliable enough. More have to develop (i.e. large time consuming and result might not be conversed to solution). Here we discuss the computation process of PDEs by FEM. Then we model an induction motor in COMSOL Multiphysics. [5] The specification of induction motor model is taken from basic design of induction motor. This model may not be implemented correctly. So we verified some characteristics and standard values. Then we reduced the turn of induction motor of one phase and observe the stator current harmonics. The harmonics in induction motor is generated by mainly stator and rotor slot if there is no manufacture defect. Other harmonics might be eccentricity harmonics, bearing fault harmonics, stator short circuit fault harmonics. In this thesis we analysis the harmonics of short circuit fault of turn. We reduced the turns for six verities and observed the results.

[4] Simulation by these tools need more determinant, proper planed, good computer system and more time consuming. Because of these reasons we have done single fault with 2-D modeling.

[5] The induction motor specifications are taken from a machine design book by A.K. Sawhney and model is verified satisfactory.

We got interesting results of induction motor stator current with faulted condition. We have analysed this faulted current in frequency spectrum.

In short our motive is to go through turn to turn fault and analysis with FEM modeling and the efficient detection process implementation

1.3 Literature Review:

Life of the induction motor can be extended by repairing before permanent damage. Most of the failure come from faults. [2] This faults occur due to some stresses namely thermal stresses, electrical stresses, mechanical stresses and environmental stresses. These stresses can be analysed in terms of different parts of the IM (i.e. stator stresses and rotor stresses). Similarly, the failures of the motor can be divided in terms of motor parts (i.e. stator failure, rotor failure). The failures of stators are mainly stator winding failure. i.e. turn to turn, coil to coil, open circuit, phase to phase, coil to ground and any combination of this. And the rotors failures are shafting, bearing, lamination, squirrel cage, ventilation system and any combination of the above.

[6] A review of Induction motor signature analysis as a medium for fault detection work is done. Where it's discussed the four faults, faults effect on stator current spectrum and fault detection techniques. The four faults are

1. Air Gap Eccentricity
2. Brocken rotor bars
3. Bearing Damage
4. Load effects

The detection Techniques are

1. Classical Fast Fourier Transform (FFT)
2. Instantaneous power FFT
3. Bi-spectrum
4. High resolution spectral analysis
5. Wavelet analysis
6. Techniques to be Associated to Motor Current Signature Analysis (MCSA)
    A. Park's Vector Approach
    B. Finite Element Method

[7] The Current Signature Analysis of Induction Motor Mechanical Faults by Wavelet Packet Decomposition (WPD) is the next step of progression of fault analysis. Here two mechanical fault are presented and experimental verification is done.

1. Bar breakage
2. Air Gap eccentricity

[3] Its presented the Modeling and Characterization of Induction Motor Internal Faults Using Finite-Element and Discrete Wavelet Transforms. Here presented two types of fault with sinusoidal and non-sinusoidal voltage source. They did not mention the user interface software of FEM. And experimental application is not done. Inter turn short circuit model is not well explained.

1. Inter turn short circuit
2. Bar breakage

[8] Electrical Fault Diagnosis for an Induction Motor Using an Electromechanical FE Model is the paper where it focused on vibration pattern for different fault conditions to diagnose the fault. Their FEM modeling is done with COMSOL Multiphisics software in 3D system. Also in this paper they did not done with experimental verification. They compared faulty conditions with healthy conditions. The faults presented.

1. Brocken Rotor Bar
2. Turn to turn

Now we are investigating the stator current for turn to turn fault with FEM implementation which are continued with next chapter.

1.4 Outline of the Thesis:

There is seven chapters in this thesis. The chapter name of 'introduction' which is studied already. Then we read the chapter of 'Finite Element Method' where we study the background of FEM, basic concept of FEM and solution of different equation by FEM. In chapter of Faults in IM we see the possibility of faults. Next chapter is 'FEM Modeling of SQIM with fault' where we read the model specifications, modeling of geometry, assignment of materials, and assignment of physics or equations and FEM mesh generation. Then we come to the chapter of 'Result and Discussion' where we see the validation of model, Individual result of each sample, method of stator current analysis and observations. Finally, we come to 'conclusion and future work' and 'reference'.

2. Chapter II

Finite Element Method

2.1 Background of Finite Element Method:

There are many theories with partial differential equations (PDE) in physics, mathematics and engineering. Solutions of these equations are more difficult by analytical method in large geometry. So there are some numerical methods are developed to solve these equations.

1. Finite Difference Method (FDM)
2. the finite volume method (FVM)
3. Boundary Element Method (BEM)
4. Finite Element method (FEM) or Finite Method Analysis (FEA)

Among these methods Finite Element Method (FEM) is more popular or well developed and simpler. The concept of this method is to consider a trial function alternative to main function and approximates the solution near to exact value. Many companies are working in this method to develop computer based codes to solve the geometry based problems. Here I have chosen the COMSOL software to solve the geometry base problems of machines like field (flux) distribution, eddy current distribution, temperature and torque distribution and so on.

2.2 The Finite Difference Method (FDM)*:*

In the field of structural analysis [9], one in every of the earliest procedures for the numerical solutions of the governing differential equations of stressed continuous solid bodies was the finite difference technique. Within the finite difference approximation of differential equations, the derivatives within the equations are replaced by difference quotients of the values of the dependent variables at separate mesh points of the domain. Once the equations are replaced by difference quotients of the values of the dependent variables at separate mesh points of the domain, once imposing the suitable boundary conditions on the structure, the separate equations are solved getting the values of the variables at mesh points. The technique has several disadvantages, as well as inaccuracies of the derivatives of the approximated solution, difficulties in imposing boundary conditions on incarnate boundaries, difficulties in accurately representing complicated geometric domains, and also the inability to utilize non-uniform and non-rectangular meshes.

2.3 The Finite Volume Method (FVM)*:*

The finite volume method [10] is a numerical method for solving partial differential equations that calculates the values of the conserved variables averaged across a volume. One advantage of the finite volume methodology over the finite difference method is that it doesn't need a structured mesh, though a structured mesh may be used. The finite volume methodology will solve problems on irregular geometries too. Moreover, yet one more advantage of the finite volume methodology over the finite element method is that it will conserve the variables on a rough mesh simply. This is an important characteristic e.g. for fluid problems.

However, the influence of finite differential method and finite volume method in solid physics is rather limited today, so that boundary element method mainly competes with finite element method in a common field, where both of these numerical methods have specific advantages.

2.4 The Boundary Element method (BEM):

The boundary element methodology [11] developed additional recently than FEM, transforms the governing differential equations and boundary conditions into integral equations that are born-again to contain surface integrals. As a result of solely surface integrals remain, surface parts are wont to perform the desired integrations. This can be the most advantage of BEM over FEM that need three-dimensional element throughout the volumetric domain. Boundary elements for a general 3 dimensional solid are quadrilateral or triangular surface elements covering the area of the element. For two-dimensional and axisymmetric issues, solely line parts tracing the define of The element is necessary.
Although BEM offers some modeling blessings over FEM, the latter will analyse additional forms of engineering applications and is way more firmly entrenched in today's computer-aided-design (CAD) surroundings. Development of engineering applications of BEM is continuing but, and additional are seen of the tactic within the future.

2.5 Finite Element Method (FEM):

2.5.1 General:

The work on Finite Element Method is started 80 years back. The work is mainly started in Russia by **Boris Galerkin**. He was a Soviet mathematician and an engineer. He took a trial function to approximate the solution of differential equation near exact solution. Idea is chosen some function whose combination would be chose to the wright answer. He has taken two or three trial functions.

Latter on the German American Mathematician **Richard Courant** introduced to choose the simplest functions to approximate the solutions.

Same idea is developed in china by mathematician **Feng Kang**.

Latter on many engineers and mathematicians works together to generate the codes to solve the differential equations by using FEM and it came to success.

2.5.2 Basic Concept:

In the finite element method of analysis, a complex region defining a continuum is discretized into simple geometric shapes called finite elements. The material properties and the governing relationships are considered over these elements and expressed in terms of unknown values at elements corners. An assembly process duly considering the loading and constraints results in a set of equations. Solution of these equations gives the approximate behavior of the continuum.
Let's try to find out the area of a circle of radius R by dividing its geometry in N number of triangle elements as Fig 2.1.

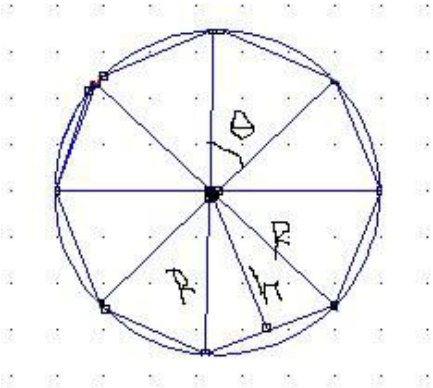

Fig.2.1: Circle with elements

Here,

$$\theta = \frac{2\pi}{N} \tag{2.1}$$

Considering any one triangle from Figure above

Base of Triangle

$$b = 2R \sin\frac{\theta}{2} \tag{2.2}$$

And height of the triangle

$$h = R \cos\frac{\theta}{2} \tag{2.3}$$

Therefore, area of this triangle

$$A_e = \frac{1}{2} bh$$

By putting the value of b and h from equation (2.2) and (2.3)

$$A_e = R \sin\frac{\theta}{2}\ R \cos\frac{\theta}{2}$$

$$= R^2 \sin\frac{\theta}{2}\ \cos\frac{\theta}{2}$$

$$= \frac{1}{2} R^2 \sin\theta$$

Now putting the value of θ from equation (2.1)

$$A_e = 0.5R^2 \sin\frac{2\pi}{N} \tag{2.4}$$

Now,

Total Area of all the triangles

$A = \sum_{e=1}^{N} A_e$

$A = NA_e$

Putting value of A_e from equation (2.4) we get,

$$A = 0.5NR^2 \sin\frac{2\pi}{N} \quad 2.5$$

Let

$\frac{2}{N} = x$

Therefore, we can rewrite the Eq. (2.5) as

$$A = \frac{R^2 \sin \pi x}{x} \quad 2.6$$

If we take infinite numbers of elements, then N→∞

So x→0 as x = $\frac{2}{N}$

For x→0

$A = \lim_{x \to 0} \frac{R^2 \sin \pi x}{x}$

By applying L'hospital's rule we get,

$A = \lim_{x \to 0} \pi R^2 \cos \pi x$

$$A = \pi R^2 \quad 2.7$$

From above we can conclude that:

1. We can divide the geometry with finite number of known elements to solve the problem. In Fig. 2.2 one arbitrary geometry is presented with triangle elements.

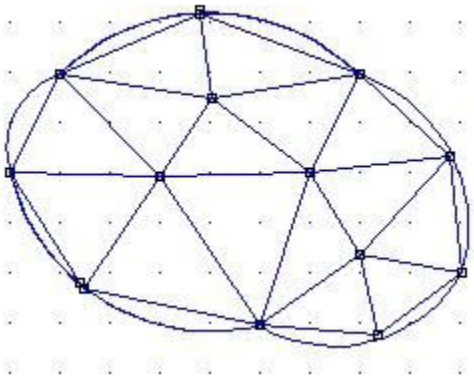

Fig. 2.2: Arbitrary geometry with elements

2. If we increase the number of elements then we get the more accurate the result or other way we can say the error will be less.

Note: Element is not bounded as triangle. There are different types of element which is shown in Fig 2.3. i.e.

a. 1D element

b. 2D elements

c. 3D elements

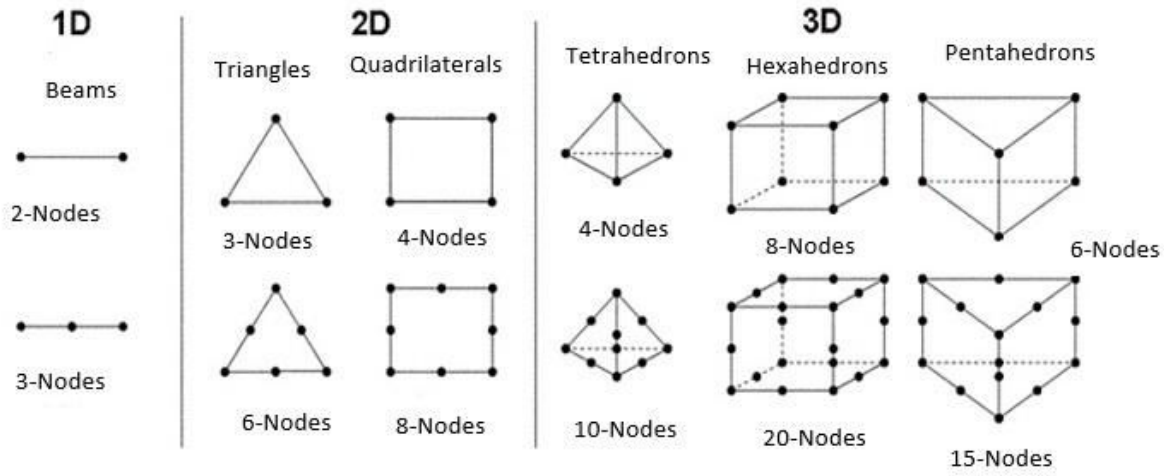

Fig.2.3: Elements in 1D, 2D and 3D

And The FEM is not about to find the area; it more about solves the problems related to

i. Mechanical stress
ii. Mechanical vibration
iii. Fatigue
iv. Motion
v. Heat transfer
vi. Fluid flow
vii. Electrostatics
viii. Electromagnetics
ix. Plastic injection moldings

From these, we are interested in electro mechanical effects which is belongs to Electromagnetics.

2.5.3 Computation process of FEM:

As an application of FEM to electrostatic problems, let us apply to solve Laplace's equation, $\nabla^2 V = 0$. Here four steps of FEM are there for solving an equation [2].

1. Finite Element Discretization
2. Element Governing Equation
3. Assembling of All Elements
4. Solving the resulting Equation

As mentioned above four steps to solve an equation, we apply these four steps to solve these Laplace's equation $\nabla^2 V = 0$.

1. Finite element Discretization:

To find the potential distribution V (x, y) for the two dimensional solution region Fig. 2.4(a), we divide the region into a number of finite elements as illustrated in Fig. 2.4(b). In Fig. 2.4(b), the solution region is subdivided into nine non-overlapping finite elements; elements 6, 8, and 9 are four-node quadrilaterals, while other elements are three node triangles. In practical situation, however, it is preferred, for ease of computation, to have elements of the same type throughout the region. That is, in Fig. 2.4(b), we could have split each quadrilateral into two triangles so that we have 12 triangular elements altogether. [9] The subdivision of the solution region into elements is usually done by hand, but in situation where a large number of elements is required, automatic schemes are used.

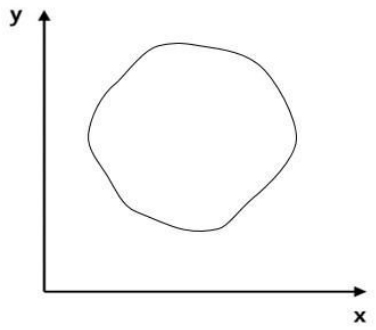

(a)

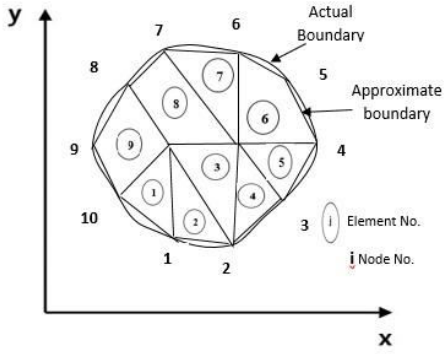

(b)

Fig. 2.4: (a) The solution region; (b) its finite element discretization

We seek an approximation for the potential $\mathbf{V_e}$ within an element **e** and then interrelate the potential distribution in various elements such that the potential is continuous across inter-element boundaries [9]. The approximation solution for the whole region is

$$\mathrm{V(x,y)} \cong \sum_{e=1}^{N} V_e(x,y) \qquad 2.8$$

Where N is the number of triangular elements into which the solution region is divided. The most common form of approximation for V_e within an element is polynomial approximation, namely,

$$V_e(x,y) = a + bx + cy \qquad 2.9$$

For a triangular element and

$$V_e(x,y) = a + bx + cy + dxy \qquad 2.10$$

For a quadrilateral element. The constants a, b, c and d are to be determined [9]. The potential V_e in general is nonzero within element e but zero outside e. In view of the fact that quadrilateral elements do not comfort to curved boundary as easily as triangular elements, we prefer to use triangular elements. Notice that our assumption of linear variation of potential within the triangular element as in Eq. (2.9) is the same as assuming that the electric field is uniform within the element [2], i.e.,

$$E_e = -\nabla V_e = -(ba_x + ca_y) \tag{2.11}$$

2. Element Governing Equations:

Considering a typical triangular element shown in Fig. 2.3. The potentialV_{e1}, V_{e2} and V_{e3} and nodes 1, 2 and 3, respectively, are obtained using Eq. (2.9), [2], i.e.,

$$\begin{bmatrix} V_{e1} \\ V_{e2} \\ V_{e3} \end{bmatrix} = \begin{bmatrix} 1 & x_1 & y_1 \\ 1 & x_2 & y_2 \\ 1 & x_3 & y_3 \end{bmatrix} \begin{bmatrix} a \\ b \\ c \end{bmatrix} \tag{2.12}$$

The coefficients a, b and c are determined from Eq. (2.12), as

$$\begin{bmatrix} a \\ b \\ c \end{bmatrix} = \begin{bmatrix} 1 & x_1 & y_1 \\ 1 & x_2 & y_2 \\ 1 & x_3 & y_3 \end{bmatrix}^{-1} \begin{bmatrix} V_{e1} \\ V_{e2} \\ V_{e3} \end{bmatrix} \tag{2.13}$$

Substituting this into Eq. (2.9) gives

$$V_e = [1 \text{ x y}] \frac{1}{2A} \begin{bmatrix} (x_2y_3 - x_3y_2) & (x_3y_1 - x_1y_3) & (x_1y_2 - x_2y_1) \\ (y_2 - y_3) & (y_3 - y_1) & (y_1 - y_2) \\ (x_3 - x_2) & (x_1 - x_3) & (x_2 - x_1) \end{bmatrix} \begin{bmatrix} V_{e1} \\ V_{e2} \\ V_{e3} \end{bmatrix} \tag{2.14}$$

Or

$$V_e = \sum_{i=1}^{3} \alpha_i(x, y) V_{ei} \tag{2.15}$$

Where

$$\alpha_1 = \frac{1}{2A}[(x_2y_3 - x_3y_2) + (y_2 - y_3)x + (x_3 - x_2)y] \tag{2.16}$$

$$\alpha_1 = \frac{1}{2A}[(x_3y_1 - x_1y_3) + (y_3 - y_1)x + (x_1 - x_3)y] \tag{2.17}$$

$$\alpha_1 = \frac{1}{2A}[(x_1y_2 - x_2y_1) + (y_1 - y_2)x + (x_2 - x_1)y] \quad 2.18$$

And A is the area of the element e, i.e.,

$$2A=\begin{vmatrix} 1 & x_1 & y_1 \\ 1 & x_2 & y_2 \\ 1 & x_3 & y_3 \end{vmatrix}$$

$$=(x_1y_2 - x_2y_1)+(x_3y_1 - x_1y_3)+(x_2y_3 - x_3y_2)$$

Or

$$A=\frac{1}{2}[(x_2 - x_1)\,(y_3 - y_1)-(x_3 - x_1)\,(y_2 - y_1)] \quad 2.19$$

The value of A is positive if the nodes are numbered counterclockwise (starting from any node) as shown by the arrow in Fig. 2.5. Note that Eq. (2.15) gives the potential

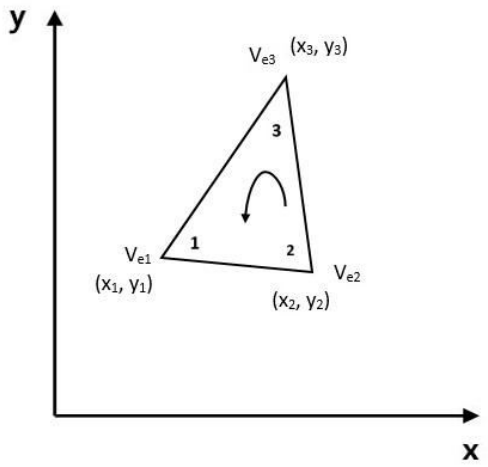

Fig. 2.5: Typical triangular element; local node numbering 1-2-3 must proceed counter-clockwise as indicated by the arrow

At any point (x, y) within the element provided that the potentials at the vertices are known. [9] This is unlike finite difference analysis, where the potential is known at the grid points only. Also note that α_i are linear interpolation functions. They are called the element shape functions and they have the following properties:

$$\alpha_i = \begin{cases} 1, & i = j \\ 0, & i \neq j \end{cases} \quad 2.20$$

$$\sum_{i=1}^{3} \alpha_i (x, y)=1 \quad 2.21$$

The shape functionsα_1, α_2 and α_3 are illustrated in Fig. 2.6.

The functional corresponding to Laplace's equation, $\nabla^2 V$=0, is given by

$$W_e=\frac{1}{2} \int \epsilon |E_e|^2 dS = \frac{1}{2} \int \epsilon |\nabla V|^2 dS \quad 2.22$$

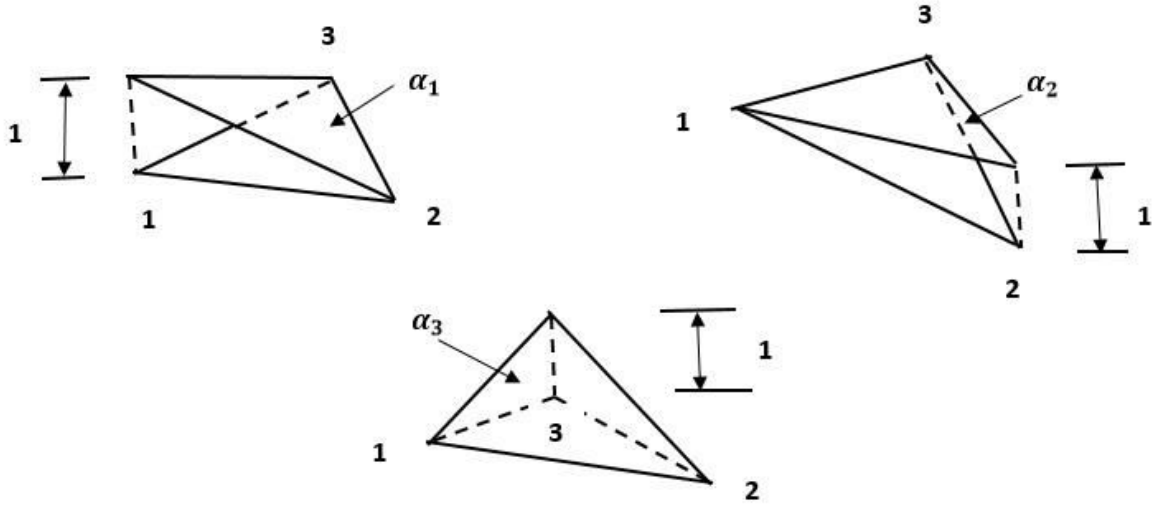

Fig. 2.6: The shape functionsα_1, α_2 and α_3 for triangular element.

(Physically, the functional W_e is the energy per unit length associated with the element e.) From Eq. (2.15)

$$\nabla V_e = \sum_{i=1}^{3} V_{ei} \nabla \alpha_i \quad 2.23$$

Substituting Equation (2.22) into Equation (2.23) gives

$$W_e = \frac{1}{2} \sum_{i=1}^{3} \sum_{j=1}^{3} \epsilon V_{ei} \left[\int \nabla \alpha_i \nabla \alpha_j dS \right] V_{ej} \quad 2.24$$

If we define the term in brackets as

$$C_{ij}^{(e)} = \int \nabla \alpha_i \nabla \alpha_j dS \quad 2.25$$

We may write Equation 2.20 in matrix form as

$$W_e = \frac{1}{2} \epsilon [V_e]^t \left[C^{(e)} \right] [V_e] \quad 2.26$$

Where superscript t means transpose of the matrix

$$[V_e] = \begin{bmatrix} V_{e1} \\ V_{e2} \\ V_{e3} \end{bmatrix} \quad 2.27$$

And

$$\left[C^{(e)}\right] = \begin{bmatrix} C_{11}^{(e)} & C_{12}^{(e)} & C_{13}^{(e)} \\ C_{21}^{(e)} & C_{22}^{(e)} & C_{23}^{(e)} \\ C_{31}^{(e)} & C_{32}^{(e)} & C_{33}^{(e)} \end{bmatrix} \quad 2.28$$

The matrix $\left[C^{(e)}\right]$ is called the element coefficient matrix or stiffness matrix in structural analysis. The element $C_{ij}^{(e)}$ of the coefficient matrix may be regarded as the coupling between nodes I and j; its value is obtained from equation (2.16), (2.17), (2.18) and (2.25) [9]

For example,

$C_{12}^{(e)} = \int \nabla\alpha_1 \nabla\alpha_2 dS$

$= \frac{1}{4A^2}[(y_2 - y_3)\ (y_3 - y_1) + (x_3 - x_2)\ (x_1 - x_3)] \int dS$

$$= \frac{1}{4A}[(y_2 - y_3)(y_3 - y_1) + (x_3 - x_2)(x_1 - x_3)] \quad 2.29$$

Similarly,

$$C_{13}^{(e)} = \frac{1}{4A}[(y_2 - y_3)(y_1 - y_2) + (x_3 - x_2)(x_2 - x_1)] \quad 2.30$$

$$C_{23}^{(e)} = \frac{1}{4A}[(y_3 - y_1)(y_1 - y_2) + (x_1 - x_3)(x_2 - x_1)] \quad 2.31$$

$$C_{11}^{(e)} = \frac{1}{4A}[(y_2 - y_3)^2 + (x_3 - x_2)^2] \quad 2.32$$

$$C_{22}^{(e)} = \frac{1}{4A}[(y_3 - y_1)^2 + (x_1 - x_3)^2] \quad 2.33$$

$$C_{33}^{(e)} = \frac{1}{4A}[(y_1 - y_2)^2 + (x_2 - x_1)^2] \quad 2.34$$

Also

$$C_{13}^{(e)} = C_{31}^{(e)}\ ,\ C_{12}^{(e)} = C_{21}^{(e)}\ ,\ C_{23}^{(e)} = C_{32}^{(e)} \quad 2.35$$

3. Assembling of All Elements :

Having considered a typical element, the next step is to assemble all such elements in the solution region. The energy associated with the assemblage of elements is [9]

$$\mathrm{W} = \sum_{e=1}^{N} W_e = \frac{1}{2}\epsilon[V]^t[C][V] \quad 2.36$$

Where

$$[\mathrm{V}] = \begin{bmatrix} V_1 \\ V_2 \\ V_3 \\ \vdots \\ V_n \end{bmatrix} \quad 2.37$$

Where, n is the number of nodes, Nis the number of elements, and [c] is called the overall or global coefficient matrix, which is the assemblage of individual element coefficient matrices. Notice that to obtain equation (2.36), we have assumed that the whole solution region is homogeneous. So that ϵ is constant. For an inhomogeneous solution region such as shown in Fig. 2.7, for example, the region is discretized such that each finite element is homogeneous. In this case, equation (2.22) still holds, but equation (2.36) does not apply since ϵ (=$\epsilon_0\epsilon_r$) or simply ϵ_r varies from element to element [9]. To apply equation (2.26), we may replace ϵ by ϵ_0 and multiply the integrand in equation (2.25) byϵ_r.

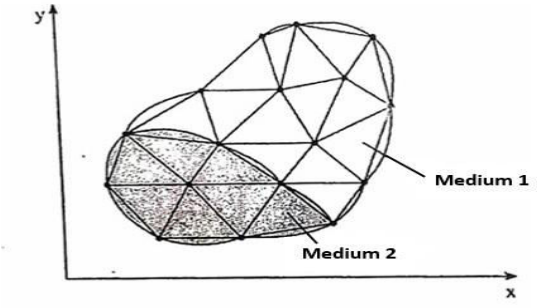

Fig. 2.7: Discretization of an in homogeneous solution region.

The process by which individual element coefficient matrices are assembled to obtain the global coefficient matrix is best illustrated with an example [9]. Consider the finite element mesh consisting of three finite elements as shown in Fig. 2.8. Observe

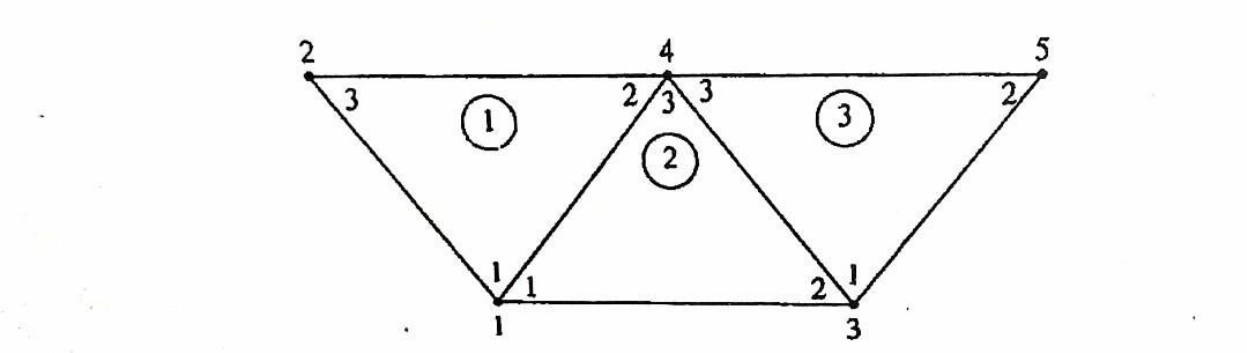

Fig. 2.8: Assembly of three elements; i-j-k corresponds to local numbering (1-2-3) of the element in Fig. 2.5.

The numbering of the mesh. The numbering of nodes 1, 2, 3, 4 and 5 is called global numbering. The numbering i-j-k is called local numbering, and it corresponds with 1-2-3 of the element in Fig. 2.5. For example, for element 3 in Fig. 2.8, the global numbering 3-5-4 corresponds with local numbering 1-2-3 of the element in Fig.2.5. (Note that the local numbering must be in counterclockwise sequence starting from any node of the element.) For element 3, we could choose 4-3-5 instead of 3-5-4 to correspond with 1-2-3 of the element in Fig. 2.5. Thus the numbering in Fig. 2.8 is not unique [2]. But whichever numbering is used, the global coefficient matrix is expected to have the form

$$[C] = \begin{bmatrix} C_{11} & C_{12} & C_{13} & C_{14} & C_{15} \\ C_{21} & C_{22} & C_{23} & C_{24} & C_{25} \\ C_{31} & C_{32} & C_{33} & C_{34} & C_{35} \\ C_{41} & C_{42} & C_{43} & C_{44} & C_{45} \\ C_{51} & C_{52} & C_{53} & C_{54} & C_{55} \end{bmatrix} \quad 2.38$$

Which is 5×5 matrix since five nodes (n=5) are involved. Again, C_{ij} is the coupling between nodes I and j. we obtain C_{ij} by using the fact that the potential distribution must be continuous across inter-element boundaries. The contribution to the I, j position in [C] comes from all elements containing nodes I and j. for example, in Fig. 2.8, element 1 and 2 have node 1 in common [9]; hence

$$C_{11} = C_{11}^{(1)} + C_{11}^{(2)} \quad 2.39$$

Node 2 belong to element 1 only; hence

$$C_{22} = C_{33}^{(1)} \quad 2.40$$

Node 4 belongs to elements 1, 2 and 3; consequently

$$C_{44}=C_{22}^{(1)}+C_{33}^{(2)}+C_{33}^{(3)} \quad 2.41$$

Nodes 1 and 4 belongs simultaneously to element 1 and 2; hence

$$C_{14}=C_{41}=C_{12}^{(1)}+C_{13}^{(2)} \quad 2.42$$

Since there is no coupling (or direct link) between nodes 2 and 3,

$$C_{23}=C_{32}=0 \quad 2.43$$

Continuing in this manner, we obtain all the terms in the global coefficient matrix by inspection of Fig. 2.8 as

$$[C]=\begin{bmatrix} C_{11}^{(1)}+C_{11}^{(2)} & C_{13}^{(1)} & C_{12}^{(2)} & C_{12}^{(1)}+C_{13}^{(2)} & 0 \\ C_{31}^{(1)} & C_{33}^{(1)} & 0 & C_{32}^{(1)} & 0 \\ C_{21}^{(2)} & 0 & C_{22}^{(2)}+C_{11}^{(3)} & C_{23}^{(2)}+C_{13}^{(3)} & C_{12}^{(3)} \\ C_{21}^{(1)}+C_{31}^{(2)} & C_{23}^{(1)} & C_{32}^{(2)}+C_{31}^{(3)} & C_{22}^{(1)}+C_{33}^{(2)}+C_{33}^{(3)} & C_{32}^{(3)} \\ 0 & 0 & C_{21}^{(3)} & C_{23}^{(3)} & C_{22}^{(3)} \end{bmatrix} \quad 2.44$$

Note that element coefficient matrices overlap at nodes shared by elements and that there are 27 term (9 for each of the 3 element) in the global coefficient matrix [C] [9]. Also note the following properties of the matrix [C]:

(1) It is symmetric ($C_{ij} = C_{ji}$) just as the element coefficient matrix [9].
(2) Since $C_{ij} = 0$ if no coupling exists between nodes I and j, it is expected that for a large number of elements [C] becomes sparse. Matrix [C] is also banded if the nodes are carefully numbered [9]. It can be shown using Eq. (2.29 to 2.34) that

$\sum_{i=1}^{3} C_{ij}^{(e)} = 0 = \sum_{i=1}^{3} C_{ij}^{(e)}$

(3) It is singular. Although this is not so obvious, it can be shown using the element coefficient matrix of Eq. (2.28) [2].

4. Solving the resulting Equations:

Using the concepts developed in chapter 4, it can be shown that Laplace's equation is satisfied when the total energy in the solution region is minimum. Thus we require that the partial derivatives of W with respect to each nodal value of the potential be Zero, [9] i.e.,

$\frac{\partial W}{\partial V_1} = \frac{\partial W}{\partial V_2} = \cdots = \frac{\partial W}{\partial V_n} = 0$

Or

$$\frac{\partial W}{\partial V_1} = 0,\ k = 1, 2, \ldots.., n \qquad 2.45$$

For example, to get $\frac{\partial W}{\partial V_1} = 0$ for the finite element mesh of Fig. 2.7, we substitute Equation (2.38) into equation (2.36) and take the partial derivative of W with respect to V_1. We obtain

$$0 = \frac{\partial W}{\partial V_1} = 2V_1C_{11}+V_2C_{12}+V_3C_{13}+V_4C_{14}+V_5C_{15}+V_2C_{21}+V_3C_{31}+V_4C_{41}+V_5C_{51}$$

Or

$$0 = V_1C_{11}+V_2C_{12}+V_3C_{13}+ V_4C_{14}+V_5C_{15} \qquad 2.46$$

In general, $\frac{\partial W}{\partial V_k} = 0$ leads to

$$0 = \sum_{i=1}^{n} V_iC_{ik} \qquad 2.47$$

Where n is the number of nodes in the mesh. By writing equation (2.47) for all nodes k = 1, 2, …., n, we obtain a set of simultaneous equations from which the solution of $[V]^t = [V_1, V_2, \ldots.., V_n]$ can be found. This can be done in two ways similar to those uses in solving finite difference equation [9, 12].

(a) Iteration Method: suppose node 1 in Fig. 2.7, for example, is a free node. From Eq. (2.46),

$$V_1 = -\frac{1}{C_{11}}\sum_{i=2}^{5} V_iC_{1i} \qquad 2.48$$

Thus, in general, at node k in a mesh with n nodes

$$V_k = -\frac{1}{C_{kk}}\sum_{i=1,i\neq k}^{n} V_iC_{ki} \qquad 2.49$$

Where node k is a free node. Since $C_{ik}=0$ if node k is not directly connected to node i, only nodes that are directly linked to node k contribute to V_k in Eq. (2.49). Equation (2.49) can be applied iteratively to all the free nodes. The iteration process begins by setting the potentials of fixed nodes (where the potentials are prescribed or known) to their prescribed value and the potential at the free nodes (where the potential are unknown) equal to zero or to the average potential

$$V_{avg} = \frac{1}{2}(V_{min} + V_{max}) \quad 2.50$$

Where V_{min} and V_{max} are the minimum and maximum values of V at the fixed nodes. With these initial values, the potentials at b the free nodes are calculated using equation (2.49). At the end of the first iteration, when the new values have been calculated for all the free nodes, they become the old values for the second iteration. The procedure is repeated until the change between subsequent iterations is negligible enough.

(b) Band Matrix Method:

If all free nodes are numbered first and the fixed nodes last, equation (2.36) can be written such that

$$W = \frac{1}{2} \in [V_f \quad V_p] \begin{bmatrix} C_{ff} & C_{fp} \\ C_{pf} & C_{pp} \end{bmatrix} \begin{bmatrix} V_f \\ V_p \end{bmatrix} \quad 2.51$$

Where subscripts f and p, respectively, refer to nodes with free and fixed (or prescribed) potentials. Since V_p is constant (it consist of known, fixed values), we only differentiate with respect to V_f so that applying equation (2.45) to (2.51) yields

$$[C_{ff} \quad C_{fp}] \begin{bmatrix} V_f \\ V_p \end{bmatrix} = 0 \quad 2.52$$

Or

$$[C_{ff}][V_f] = -[C_{fp}][V_f] \quad 2.53$$

This equation can be written as

$$[A][V] = [B] \quad 2.54$$

Or

$$[V] = [A]^{-1}[B] \quad 2.55$$

(2.39b)

Where $[V] = [V_f]$, $[A] = [C_{ff}]$, $[B] = -[C_{fp}][V_p]$. Since [A] is, in general, nonsingular, the potential at the free nodes can be found using equation (2.54, 2.55). We can solve for [V] in

equation (2.54) using Gaussian elimination technique. We can also solve for [V] in equation (6.55) using matrix inversion if the size of the matrix to be inverted is not large.

It is sometimes necessary to impose Neumann condition ($\frac{\partial V}{\partial n} = 0$) as a boundary condition or at the line of symmetry when we take advantage of the symmetry of the problem. Suppose, for concreteness, that a solution region is symmetric along the y-axis as in Fig. 2.9. We impose condition ($\frac{\partial V}{\partial x} = 0$) along the y-axis by making

$$V_1 = V_2,\ V_4 = V_5, V_7 = V_8 \qquad 2.56$$

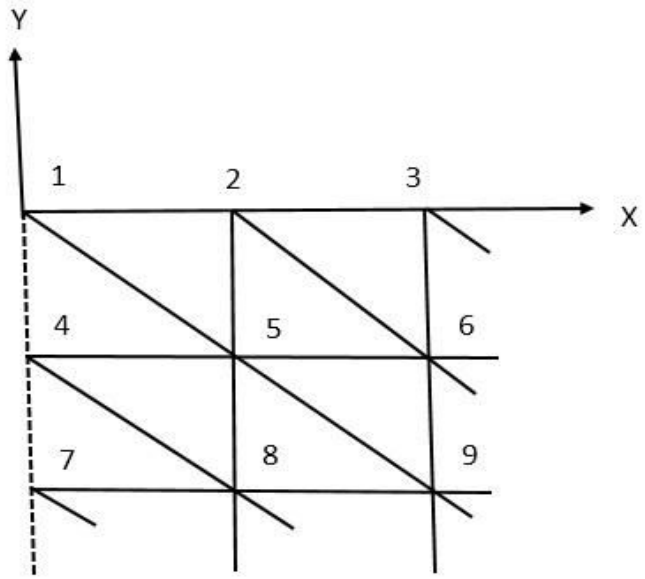

Figure 2.9: A solution region that is symmetric along the y-axis

Notice that as from equation (2.22) onward, the solution has been restricted to a two- dimensional problem involving Laplace's equation, $\nabla^2 V = 0$.

2.6 Software introduction to implement the FEM:

Many Companies develops software to implement the FEM in different geometry. **ANSYS**, **COMSOL Multiphysiscs, BAQUS** and **ALGOR** are the example of software tool which can use to study the electromagnetics. As per suggestion from teachers and seniors the COMSOL is the most useful and simpler software tool with more nodes/elements. So I have started to learn the COMSOL and I am able to modeling and result analysis. I have done with modeling of Rotating Machinery and induction motor which are given following chapters. One more basic software tool is there name as **FEMM.**

3. Chapter III

Faults in Induction Motor

3.1 Induction Motor:

Alternating current, or AC motors provide much of the motive force for industry. AC motors are available a spread of designs and power ratings. AC motors are sometimes designed to be used with fixed input voltage signals. These motors are also classed as low, medium and high voltage. Low voltage motors sometimes consume between regarding 240V and 600V. Medium voltage motors consume voltages from regarding 400V up to about 15kV. [1, 5, 12] High voltage motors consume voltage over 15kV. AC motors employed in industrial applications are sometimes synchronous motors having a beginning winding and a running winding. [1, 5, 12] The beginning winding includes a starting condenser or different electrical phenomenon part nonparallel with the winding to shift the part of the voltage and therefore the current applied to the starting winding with relevance the voltage and the current applied to the running winding. AC motors are employed in a spread of applications, together with vehicle applications like traction management. Traction motors are giant electrical motors having the standard motor housing, mechanical device and rotor assembly. Shaft is connected to the rotor that extends through the housing. Fixed connected to a pinion finish of the shaft may be a motor pinion that successively engages a bull or shaft gear for rotating the axle. The motors employed in vehicle applications are sometimes controlled specified the motor section currents are curving. These motors are usually static magnet motors designed to possess a sinusoidal-shaped back magnetism field wave form. Associate induction motor is employed as a motor. [1, 5, 12] The terminal voltage of the induction motor includes a transient voltage drawn by the merchandise of the differentiation term of a primary current and therefore the discharge inductance of the induction motor. A good style of induction motors is obtainable and are presently in use throughout a variety of business applications. Induction motors sometimes embody a rotor that rotates in response to a rotating magnetic flux generated by the electrical energy in a very stator coil related to the rotor. A motion speed differential between the rotor and therefore the rotating flux induces a current through a rotor cage. A rotor cage consists of one aluminum casting having many semi conductive bars that run axially through the rotor and are joined at every finish by 2 conductive end rings. Current iatrogenic within the bars generates a magnetic flux that opposes that of the mechanical device, therefore providing the rotor with movement torsion. [1, 5, 12] The mechanical device and also the rotor could also be automatically and electrically organized in a very type of manners relying upon variety of things, including: the applying, the ability obtainable to drive the motor, then forth.

The induction motors are divided once more into an inner rotor sort induction motor and an outer rotor type induction motor in accordance with relative positions of rotors and stators. The inner rotor sort induction motor is mostly applied to a washer or one thing like that, and includes the rotor within the stator coil. The flexibility to accurately verify the speed of a rotating rotor with

relation to a stationary stator coil inside an induction motor is vitally vital to the everyday operations of induction motors.
A flat induction motor could be a motor that includes a disk-shaped mechanical device and rotor placed coaxially around a rod with their surfaces opposing one another. Normally, each the stator core and the rotor core have a spiral winding structure made of a magnetic steel strip. A plurality of open slots is shaped within the winding structures from the border toward the rod at equal intervals, departure a part of the magnetic steel strips.
[1,5,12] Single part induction motors are commonly given a cage kind rotor and a spiraling stator coil having 2 windings, one being for the running coil and therefore the different for the beginning coil. Single phase induction motors are wide used, for their simplicity, strength and high performance. [1,5,12] They're employed in social unit appliances, like refrigerators, freezers, air conditioners, tight compressors, laundry machines, pumps, fans, moreover as in some industrial applications
[1, 5, 12] Linear induction motors are wide employed in variety of industries and gift bound benefits over rotary motors, notably wherever propulsion on a preset path or guide or guide way is required.

3.2 Type of faults:

[2] We have already seen in literature review that the fault may occur in induction motor due to thermal, electrical, mechanical and environmental stresses. There are four major faults which may occur are below.

1. Short circuit fault in stator
2. Rotor bar and ring fault
3. Bearing fault
4. Air-gap eccentricity fault

3.3 Short circuit fault:

[19] In normal operation of industrial motors, there is usually 10 to 100V (AC) between the adjacent turns in a coil. The insulation is about 0.5mm thick as the voltage across the turn insulation is relatively low. However, substantial transient voltages across the turn insulation are possible during switching operations. Majority of motor stator winding failure happens due to the destruction of the turn insulation caused by the short circuit in stator windings. The type of shorts could be of the following types:

i. Inter-turn shorts of same phase
ii. Short between coils of same phase
iii. Short between two phases
iv. Short between phases to earth
v. Open circuit fault

Fig. 3.1 shows the schematic diagram of the different types of stator winding problems. Several studies [17-24] report that depending on the type of shorts, and condition of motor (age, working condition, etc.), the motor may continue to operate initially, even though short-circuit current will flow, causing more and more overheating, ultimately leading to complete failure if not accounted

for. The studies [17-24] also point that with the inter-turn and coil short of same phase, the motor might still continue to run. The detrimental ones are the short between the phases and phase-to-earth, causing instantaneous motor shutdown. About the failure mode trend, it is generally argued that the shorts in a particular phase, if undetected, would grow onto phase to- phase faults. Although there are no exclusive data to indicate the transition time between inter-turn (in same phase) and ground wall (between phase-to-phase) insulation failure [20], however, detection of inter-turn shorts during motor operation would reduce the damage to adjacent coils and the stator

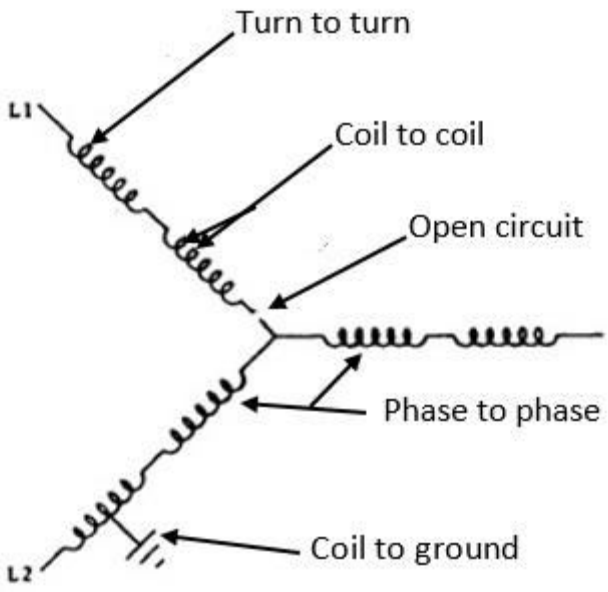

core, reducing repair cost and motor outage time.

Fig. 3.1: Possible failure Modes of Y-connected Stator

3.4 Rotor bar and ring Fault:

If the rotor cage is healthy, the magnetic stress around the rotor is symmetric, and as a result, the resultant magnetic force is zero. [25] However, in the case of broken rotor bars or broken ring, magnetic asymmetry produces an unbalanced magnetic force, which is rotating at the rotational frequency and modulated with a frequency equal to the slip frequency times the number of poles. This causes the vibration in the motor. Which may cause the failure of bearing or shaft.

3.5 Bearing Fault:

The typical geometric structure of a rolling-element bearing is shown in Fig. 3.2 Rolling-element bearings are mainly composed of the outer and inner raceway, the ball elements, and the cage, which ensures the distances between the ball elements uniformly. [26] On ordinary conditions,

bearing faults can be separated into two types, that is, single-point (also called localized or cyclic) and generalized-roughness (also called distributed or noncyclic) faults. [27, 26] Localized faults could be imagined as a small hole, a pit, or a missing piece of material and they affect a localized region. [27] When a localized defective bearing runs at a constant speed, a periodic impact between rolling elements and the raceway is produced. The existence of such impulsive forces gives rise to an increase in the vibration level. The characteristic frequencies of these vibrations rely on fault location, bearing geometry, and operating speed. Not alike localized faults, generalized-roughness faults greatly worsen the entire area of a bearing element because of the absence of lubrication, erosion, or bearing pollution and are hard to represent by specific frequencies.

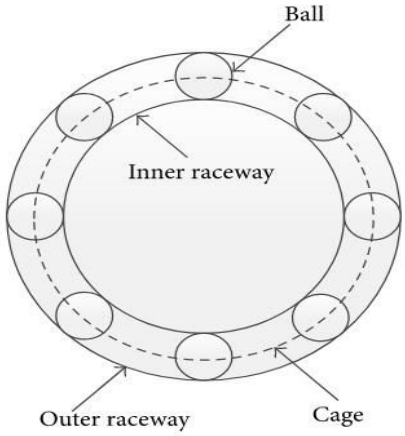

Fig. 3.2: Typical structure of a rolling-element bearing with main parameters

Localized faults can be usually divided into four categories depending on the affected element, namely,

1. outer raceway fault
2. inner raceway fault
3. ball fault, and
4. cage fault

3.6 Air gap eccentricity fault:

This fault may present due to manufacture defect, bearing fault, bar and ring fault, etc. Radial air gap of the motor will be differed due to eccentricity fault. This fault is two type namely, static and dynamic eccentricity.

1. Static eccentricity fault

Normally, the rotor that is centered at the stator bore of healthy motor results in identical air-gap among the stator and rotor. [28] Accordingly, the magnetic forces are balanced in the opposite directions, but when the eccentricity emerges, this air-gap lessens on one side whereas it increases

on the other side at any gyration angle which causes higher absorption force through the shorter gap

[28] Static eccentricity in electrical motors occurs when the rotor symmetrical axis is concentric with the rotor rotational axis; however, they are dislocated with respect to the stator symmetrical axis; hence, the position of minimum radial air-gap length is fixed. In this situation the mutual inductances across the stator and rotor as well as the self- and mutual inductances between the rotor phases are a function of rotor angular position. [28] The self- and mutual inductances among the stator phases are invariant and independent of the rotor angular position, same as healthy condition of motor.

2. Dynamic eccentricity fault

In the SE, the rotor is displaced from the stator center, but the rotor rotates around its own center. In the DE, the rotor is also displaced from the stator center, but the rotor rotates around the center of the stator center.

4. Chapter IV

FEM Modeling of Squirrel Cage Induction Motor

4.1 The work definition:

To work with FEM Modeling we have designed the following motor using conventional design process:

Specifications: Design 2.2 kW, 400V, 3-phase, 50 Hz, 1500 synchronous r.p.m. squirrel cage induction motor. The machine is to be started by a started by a star delta starter. The efficiency is 0.8 and power factor is 0.825 at full load.

The design summary is as follows,

Rating:

1. Full load output = 2.2 kW
2. Line voltage = 400 V
3. Frequency = 50 Hz
4. Phases = 3
5. Efficiency = 0.8
6. Power factor = 0.825
7. Number of poles = 4
8. Synchronous r.p.s. = 25
9. kVA input = 3.33
10. Full load line current = 4.8

Loading:

1. Specific magnetic loading = 0.44 Wb/m^2
2. Specific electric loading = 21000 A/m
3. Output co-efficient = 97
4. $D^2L = 1.375 * 10^{-3}\ m^3$

Main Dimensions:

1. Stator bore = 105 mm
2. Gross iron length = 125 mm
3. Ducts = Nil
4. Net iron length =112.5 mm
5. Pole pitch = 82.9 mm

Stator:

1. Type of laminations = 0.5 thick lohys
2. Type of winding = single layer mush

3. Connection = Delta
4. Phase voltage = 400 V
5. Flux per pole 4.54 * 10^{-3}Wb
6. Turns/phase = 416
7. Number of slots = 24
8. Slots per pole = 6
9. Slots per pole per phase = 2
10. Coil span = 5 slots
11. Distribution factor = 0.966
12. Pitch factor = 0.9659
13. Winding factor = 0.934
14. Slot pitch = 13.75 mm
15. Conductor/slot = 104
16. Conductor bare diameter = 0.95 mm
17. Conductor insulated diameter = 1.041 mm
18. Conductor area = 0.709 mm^2
19. Current density = 3.91 A/mm^2
20. Length of mean turn = 0.68 mm
21. Phase resistance at 75 ^{0}C = 8.37 Ohm
22. Copper loss at full load = 193 W
23. Depth of stator core = 17 mm
24. Outer diameter stator laminations = 181mm

Stator slot Dimension:

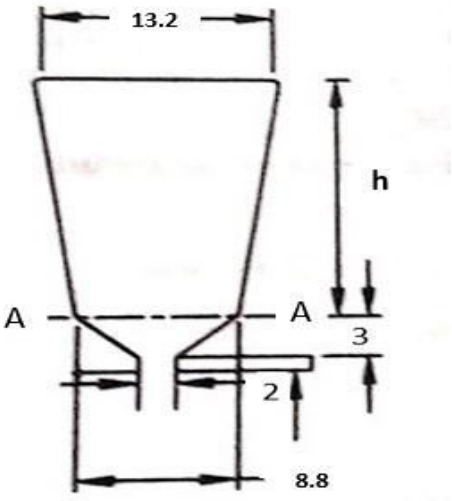

Fig. 4.1: stator slot dimensions (in mm)

1. Area of each slot = 184 mm^2
2. The maximum allowable flux density of teeth = 1.7 wb/m^2

3. Flux d4ensity in stator teeth = 1.12 Wb/m^2
4. Take lip = 1 mm
5. Wedge = 3 mm
6. Slot width at AA = 8.8 mm
7. Height of slot (h) = 17 mm
8. Depth of the slot = 21 mm

Rotor:

1. Length of air gap = 0.3 mm
2. Diameter of rotor =104.4 mm
3. Type of winding = squirrel cage
4. Number of slot = 22
5. Slot/pole/phase = 1.835
6. Conductor per slot = 1
7. Winding factor = 1
8. Slot pitch = 14.9 mm
9. Rotor bar current = 244 A
10. Rotor bar cross section = 7 * 6.5 mm
11. Rotor bar area = 44.6 mm^2
12. Rotor bar length = 165 mm
13. Rotor bar current density = 5.47 A/mm^2
14. Resistance of each bar = 77.7 * 10^{-6} Ohm
15. Copper loss in bar = 101 W
16. End ring current = 428
17. End ring cross section = 10 * 8 mm
18. End ring area = 80 mm^2
19. End ring main diameter = 75.8 mm
20. End ring current density = 5.35 A/mm^2
21. Resistance of each ring = 62.8 * 10^{-6} Ohm
22. Copper loss in end ring = 23 W
23. Total rotor copper loss = 124
24. Resistance of rotor (referred to stator) = 7.83 Ohm
25. Depth of rotor core = 17 mm

Rotor slot:

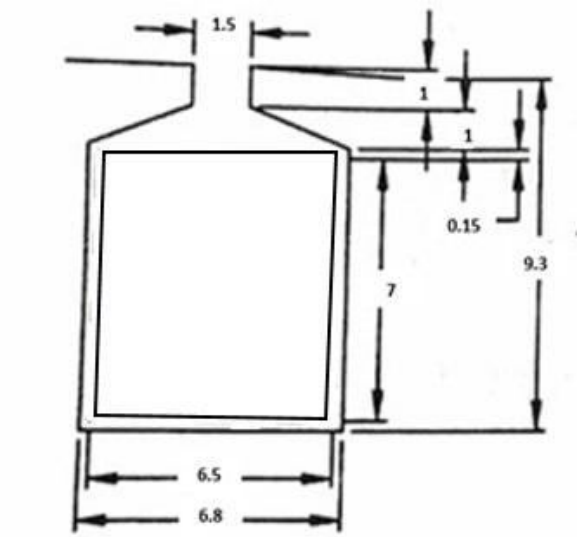

Fig. 4.2: rotor slot dimensions (in mm)

No load current:

1. Magnetizing mmf/pole = 231 A
2. Phase magnetizing current = 1.0 A
3. Magnetizing reactance = 400 Ohm
4. Core loss = 134 W
5. Friction and wind age loss = 33 W
6. No load loss = 167 W
7. Loss component = 0.139 A
8. No load current (phase) = 1 A
9. No load current (Line) = 1.73 A
10. No load power factor = 0.139

Short circuit (blocked rotor) current:

1. Slot leakage reactance 11.8 Ohm
2. Overhang leakage reactance = 4.7 Ohm
3. Zigzag leakage reactance = 20.3 Ohm
4. Total leakage reactance = 36.8 Ohm
5. Total resistance = 16.2 Ohm
6. Short circuit impedance = 40.2 Ohm
7. Phase short circuit current = 9.95 A
8. Line short circuit current = 17.5 A
9. Short circuit p.f. = 0.043

Performance:

At full load

1. Losses = 484 W
2. Output = 2200W
3. Input = 2684 W
4. Efficiency = 81.3%
5. Power factor = 0.829
6. Slip = 5.3%
7. Maximum power output/rated output = 1.67
8. Maximum torque/rated torque = 2
9. Starting torque/rated torque = 1
10. Temperature rise = 45.6 ^{0}C

4.2 FEM Modeling:

We modeled the motor by COMSOL Multiphysics in 2D system. This model simulates the electro-mechanical effects in a three phase squirrel cage induction motor. The assembly consists of stator and rotor. Induction motor simulated is constructed as 24 stator slots, 22 rotor slots, and four pole machine. The mechanical dimensions which is mentioned in starting of this chapter are used to model the geometry of the squirrel cage induction motor. We defined the physics, mesh generation and solved in time domain. The simulation process is shown in flow chart in below and important parts are discussed.

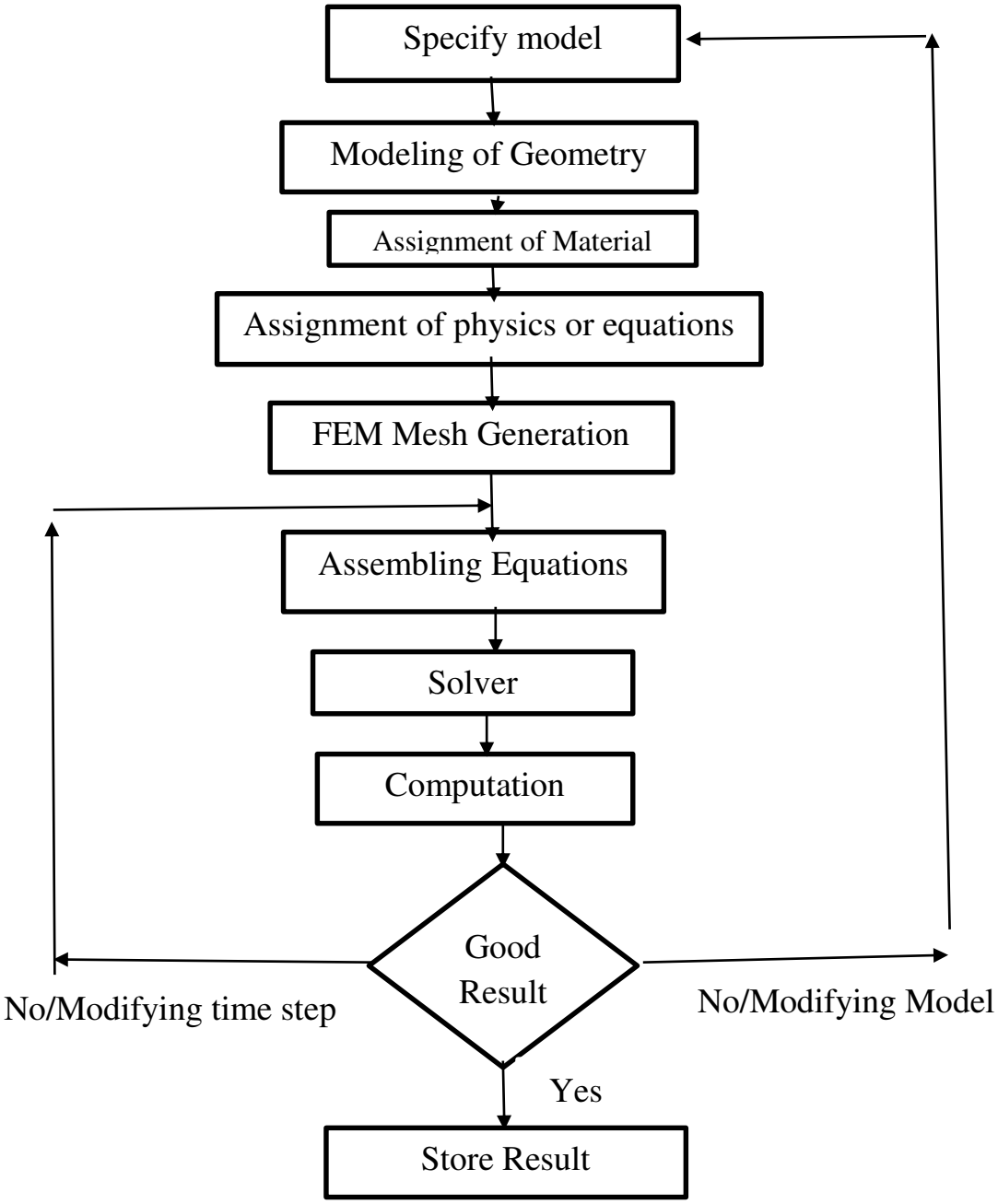

4.3 Model specification:

Firstly, in the model specification phase, the model of the problem, which simulation require electromagnetic field calculations must be set up, i.e. we have to design induction motor or collect the required design dimensions and find out the partial differential equations, which must be solved with prescribed boundary and continuity conditions.

4.4 Modeling of Geometry:

Here we taken some dimensions of the squirrel cage induction motor from theoretical design. Some important dimensions are mentioned below which is applied here and The Modeled geometry corresponds to these dimensions (in Fig. 4.3)

Serial Number	Induction Motor Parameter		
	Parameters	Value	Units
1	Length of the motor	112.5	mm
2	Outer diameter of the stator	181	mm
3	Inner diameter of the Stator	105	mm
4	Number of stator slot	24	
5	Number of Turns	1248	
6	Outer diameter of rotor	104.4	mm
7	Number of Bars	22	
8	Air Gap	0.3	mm
9	Number of pole	4	

Table 4.1: Some dimensions of SCIM

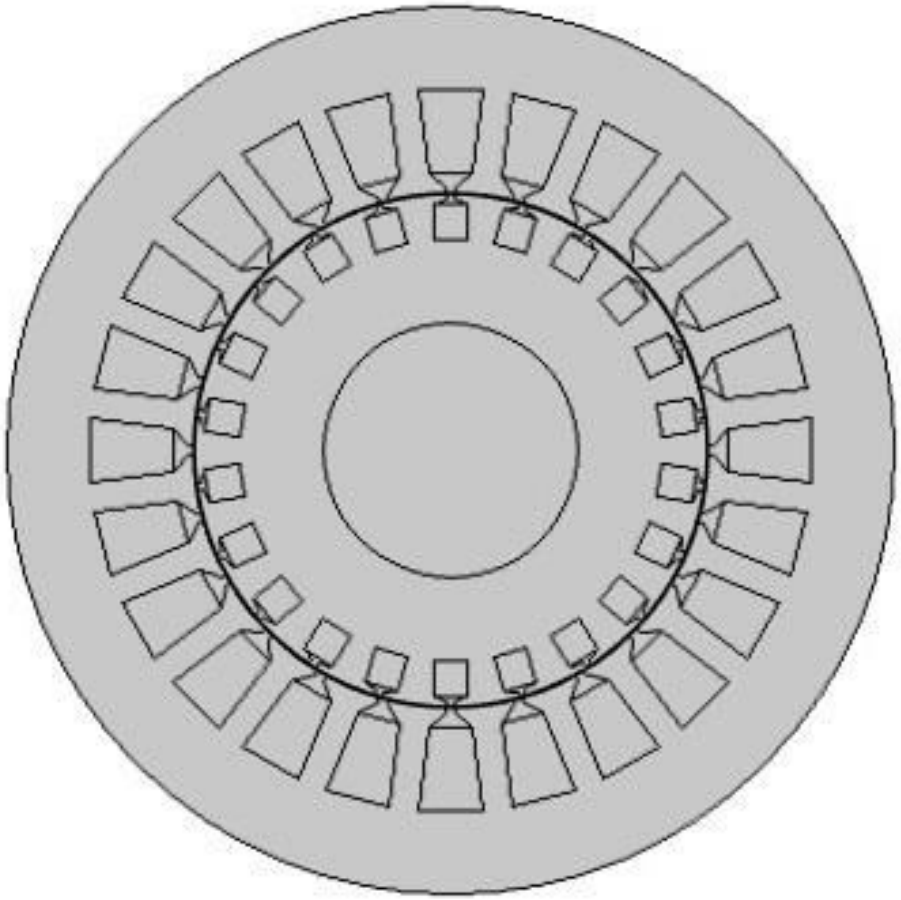

Fig. 4.3: Geometry of squirrel cage IM in 2D

4.5 Assignment of Materials:

[5] Defining of material is an important thing to be done. And every property of the material should be provided correctly i.e. conductivity, relative permeability, relative permittivity etc. Materials assigned to various sectors of motor under consideration are air gap as air, rotor core sector and shaft are defined as steel, bar as copper. Here we used bar material as copper instead of aluminium as designed.

4.6 Assignment of physics or Equations:

This is the most complex to understand the equations and implement in right way in COMSOL Multiphysics. It is relatively modest to employ the magnetic vector potential in the numerical solution of the field the induction motor since its simplicity to represent the magnetic fields as a two-dimensional model. Due to complex structure of induction motor, fields of the machine are clearly three dimensional, that's why a two-dimensional solution is always close approximation. The equations are given below which are applied to the FEM model.

A. Maxwell Equations:

Let us start with the application of full three-dimensional vector equations.

The magnetic vector potential A is given by

$$B = \nabla \times A \tag{4.1}$$

Coulomb's condition, required to define explicitly the vector potential, is written as

$$\nabla \cdot A = 0 \tag{4.2}$$

The substitution of the definition for the magnetic vector potential in the induction law yields

$$\nabla \times E = -\nabla \times \partial A/\partial t \tag{4.3}$$

Electric field strength can be expressed by the vector potential A and the scalar electric potential φ as

$$E = -\partial A/\partial t - \nabla\varphi \tag{4.4}$$

' ϕ ' is the reduced electric scalar potential.

Since $\nabla \times \nabla\varphi \equiv 0$, adding a scalar potential causes no problems with the induction law. Above equation gives that the electric field strength vector comprises of two parts, they are a rotational part induced by the time dependence of the magnetic field, and a non-rotational part produced by electric charges and the polarization of dielectric materials.

Current density depends on the electric field strength.

$$J = \sigma E = -\sigma\, \partial A/\partial t - \sigma\nabla\varphi \tag{4.5}$$

Ampere's law and the definition for vector potential gives

$$\nabla x\,(1/\mu\, \nabla x\, A) + \sigma\, \partial A/\partial t + \sigma\nabla\varphi = 0 \tag{4.6}$$

By substituting equation (5) into (6) gives

$$\nabla x\,(1/\mu\, \nabla x\, A) = J \tag{4.7}$$

Equation (4.7) is valid in zones where eddy currents may be induced, while the equation (4.6) is valid in zones with source currents J = Js, such as stator or rotor winding currents, and in zones without any current densities usually J = 0.

In electrical machines of any type, a 2D solution is often the apparent one as in [1]; in these cases, the numerical solution can be deduced based on a single component of the vector potential A. The solution for fields B, H are found in an x-y plane, whereas J, A and E involve only the z-component. The gradient ∇φ has a z-component, since J and A are parallel to z, and equation (4.5) is effective. The summarized scalar potential is thus independent of x- and y-components. 'φ' could be a linear

function of the z-coordinate, since a 2D field solution is independent of z. The assumption of two-dimensionality is not valid for potential differences caused by electric charges or by the polarization of insulators. For two-dimensional cases with eddy currents, the scalar potential has to be set as φ = 0.

In a 2D case, the equation (4.6) is rewritten as

$$\nabla . (1/\mu \nabla Az) + \sigma \partial Az/\partial t = 0 \quad 4.8$$

Exterior of the eddy current zones, below equation is more valid:

$$-\nabla . (1/\mu \nabla Az) = Jz \quad 4.9$$

The definition of vector potential provides below components for flux density:

$$Bx = \partial Az/\partial y;\ By = -(\partial Az)/\partial x \quad 4.10$$

Therefore, the vector potential remains constant in the direction of the flux density vector.

In the 2D case, the below equation can be obtained from the partial differential equation (PDE) of the vector potential:

$$-k[\frac{\partial}{\partial x}\left(v\frac{\partial Az}{\partial x}\right)+\frac{\partial}{\partial y}\left(v\frac{\partial Az}{\partial x}\right)] = kJ \quad 4.11$$

Where 'ν' is the reluctivity of the material above equation is exactly similar to the equation of a static electric field.

$$\nabla \cdot (\nu \nabla A) = -J \quad 4.12$$

B. Boundary conditions:

Definition of two types of boundary conditions for this type of 2D problems is valid. First, Dirichlet's boundary condition indicates that a known potential, so that vector potential

$$A = \text{constant} \quad 4.13$$

This can be attained for a vector potential for example on the outer surface of an electrical induction machine. Since the field is parallel to the contour of the surface. Same as the outer surface of an electrical induction machine, the center line of the machine's pole can develop a symmetry plane. Neumann's homogeneous boundary condition determined with the vector potential

$$\partial \mathrm{A}/\,\partial \mathrm{n} = 0 \qquad 4.14$$

is a second boundary condition accomplished at an instance the field meets a contour perpendicularly. In equation (4.14) 'n' is the normal unit vector of a plane. A contour of this kind is part of a field confined to infinite permeability iron as shown in figure.4.4. The magnetic flux piercing a surface is easy to determine with the vector potential. Stake's theorem develops the flux equation.

$$\emptyset = \int_s [B.dS] = \int_s [(\nabla \times \mathrm{A}).dS] = \int_l [A.dl] \qquad 4.15$$

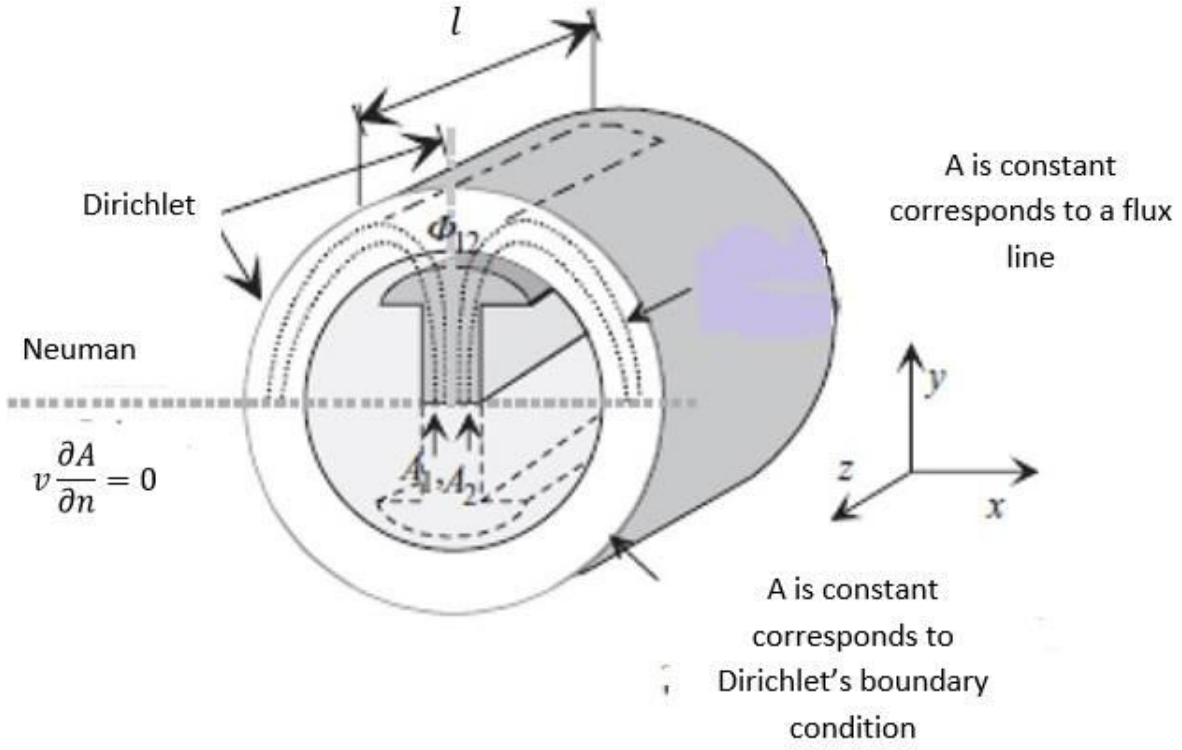

Fig. 4.4: Definition of boundary condition

Flux 'Φ' is an integral around the contour 'l' of the surface S as illustrated in the fig.4.4. In the 2D case of the illustration [5], the end faces' part of the integral is zero and the vector potential along the axis is constant.

Consequently, for an induction machine of the length 'l' we obtain a flux

$$\Phi 12 \; = \; \mathrm{l}\,(\mathrm{A1} \; - \; \mathrm{A2}) \qquad 4.16$$

This represents that the flux Φ12 is the flux between vector equipotential lines A1 and A2.

C. Arkkio's Torque:

Applying finite element assumptions, torque can be determined by differentiating the magnetic co energy W1 with respect to movement, and by maintaining the winding current constant:

$$T = l\frac{dW^1}{d\alpha} = \frac{d}{d\alpha}\int_v \int_0^H [(B.dH)dV] \tag{4.17}$$

In numerical modeling, this air-gap magnetic field energy and torque produced due to it is approximated by the difference between two successive fields.

$$\mathrm{T} = [l\left(\mathrm{W'}(\alpha + \Delta\alpha) - \mathrm{W'}(\alpha)\right)]/\Delta\alpha \tag{4.18}$$

Where 'l' is the machine length and Δα represents the displacement between successive field solutions.

There are four different methods to calculate torque of rotating electrical machines using FE modeling; they are Coulomb's method, Maxwell Tensor method, Magnetic co energy derivation and Arkkio's method. Among them Arkkio's method [13] is used in this work to determine torque of IM using FEM. It is a variant of Maxwell's stress tensor method and is based on integrating the torque over the whole volume of the air gap constituted by the zones of radii r_r and r_S. Torque expression of same is as shown below (4.19).

$$T = \frac{l}{\mu_0(r_s - r_r)}\int_s r\, B_n B_{tan}\, dS \tag{4.19}$$

Where l is the length, B_n and B_{tan} represents the radial and tangential flux densities in the elements of surface S and formed between radii r_r and r_s, dS is the surface of single element**.**

D. Simplified Electrical Circuit:

Into motor model, an electrical circuit is implemented which includes sinusoidal voltage source to feed the motor, end winding impedance and an external coupling to provide a connection to the Rotating Machinery. For one stator phase, the electrical circuit is shown in Fig. 4.5 for which Kirchhoff's voltage law is defined:

$$V = R_{Send}i + L_{Send}\frac{di}{dt} + V_{emf} \tag{4.20}$$

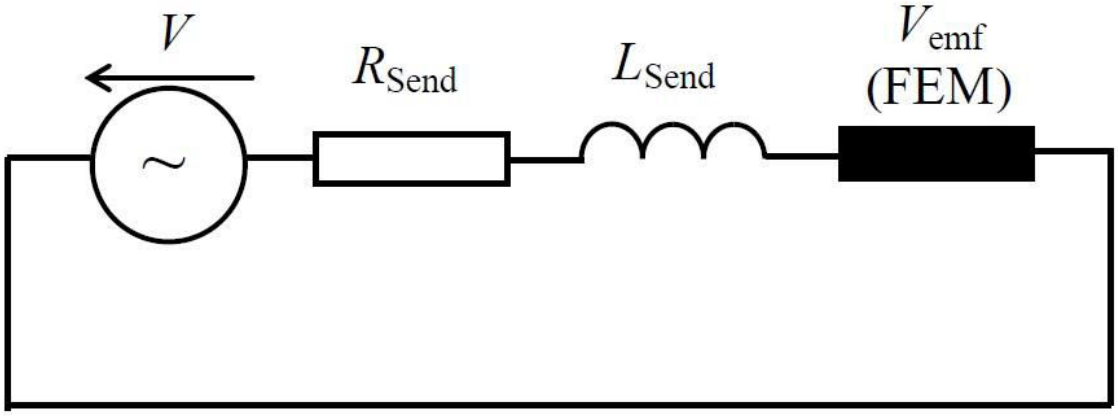

Figure.4.5 External stator electrical circuit for one phase.

Where V is the phase voltage in (V), i is the current in the loop in (A),

R_{Send} is the resistance of the stator winding overhang in (Ohm) [1, 5]

$$R_{Send} = \rho \frac{2l_0 N_S}{A} \tag{4.21}$$

Where ρ is the resistivity in (Ohm. m), l_0 is the mean length of the stator winding overhang in (m), N_s is the number of turns per one stator phase, [1,5] A is the cross-section area of the stator winding conductor in (m^2).

L_{Send} is the leakage inductance of the stator winding overhang in (H)

$$L_{Send} = \frac{2l_0 \mu_0 \lambda_0 N_S^2}{p} \tag{4.22}$$

Where

$$\lambda_0 = k_o(1 - 0.64\frac{y}{l_0})q \tag{4.23}$$

[1,5] Where k_0 is the factor depending on the type of the stator winding, y is the coil span in (m), q is the number of slots per pole and per phase, p is the number of pole pair and μ_0 is the absolute permeability [1,5].

V_{emf} are the induced voltages in (V) across the sides of the all stator coils in one phase, which are implemented in the Rotating Machinery, Magnetic interface.

A part of external rotor electrical circuit is in Fig. 4.6.

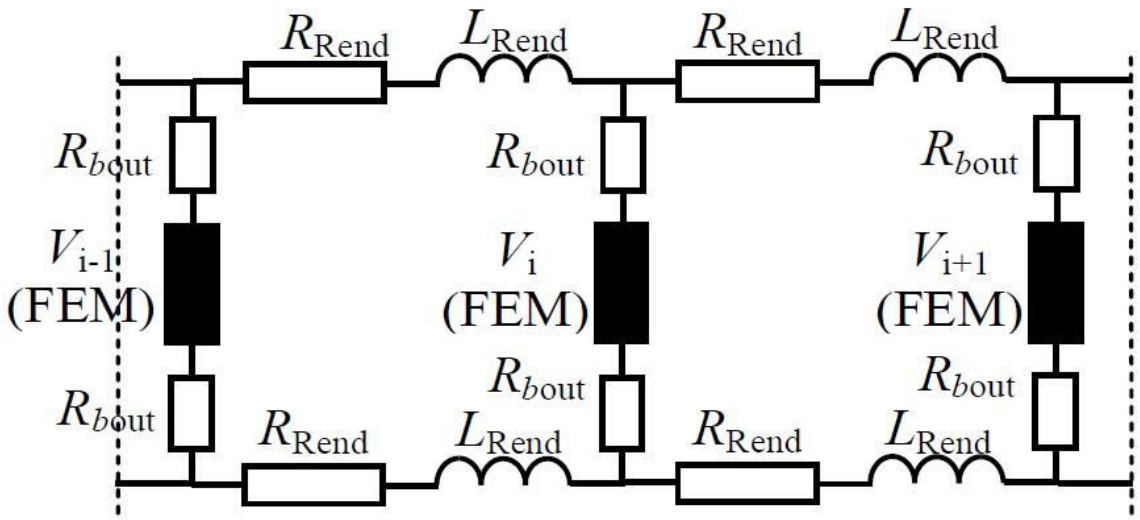

Figure 4.6: External rotor electrical circuit for one phase**.**

The voltage equation for one loop of the rotor electrical circuit in Fig. 4.6 defined by Kirchhoff's voltage law is as follows:

$$v_i - v_{i+1} = 2R_{bout}i_{bi+1} + 2R_{Rend}i_{Ri} + 2L_{Rend}\frac{di_{Ri}}{dt} \tag{4.24}$$

where v_i, v_{i+1} are the voltages of two neighboring bars in (V), which are implemented in the Rotating Machinery, Magnetic interface, i_{bi}, i_{bi+1} are the currents in the bars in (A), i_{Ri}, i_{Ri+1} are the currents in the rings in (A),

R_{bout} is the resistance of the part of bar, which is outside of the rotor iron in (Ohm)

$$R_{bout} = \rho\frac{l_{bout}}{A_b} \tag{4.25}$$

Where l_{bout} is the mean length of the bar outside of the iron sheets in (m), A_b is the cross section area of the bar in (m^2).

R_{Rend} is the resistance of the rotor end-ring segment in (Ohm)

$$R_{Rend} = \rho\frac{\pi d_{RN}}{QA_R} \tag{4.26}$$

Where d_{RN} is the mean diameter of the cage end ring in (m), Q is the number of rotor bars, A_R is the cross section area of the cage end ring in (m^2).

L_{Rend} is the leakage inductance of the rotor end-ring segment in (H)

$$L_{Rend} = \mu_0 \frac{\pi d_{RN}}{Q} \lambda_{Ro} \quad 4.27$$

Where

$$\lambda_{Ro} = \frac{Q}{2 m_S p l_0} \tau_p g \quad 4.28$$

Where m_S is the number of stator phases, τ_p is the pole pich, g is the factor defined in [5].

The parameters R_{bout}, R_{Rend} and L_{Rend} are defined in [5].

4.7 FEM Mesh Generation:

In the pre-processing task the geometry of the problem must be discretized by a finite element mesh. The fundamental idea of FEM is to divide the problem region to be analysed into smaller finite elements with given shape. A finite element can be triangles or quadrangles in two dimensions.

A triangle (Fig. 4.7(a)) has three vertices 1, 2 and 3, here numbered anticlockwise and has 3 edges. The quadrangle element (Fig. 4.7(b)) has 4 nodes and 4 edges.

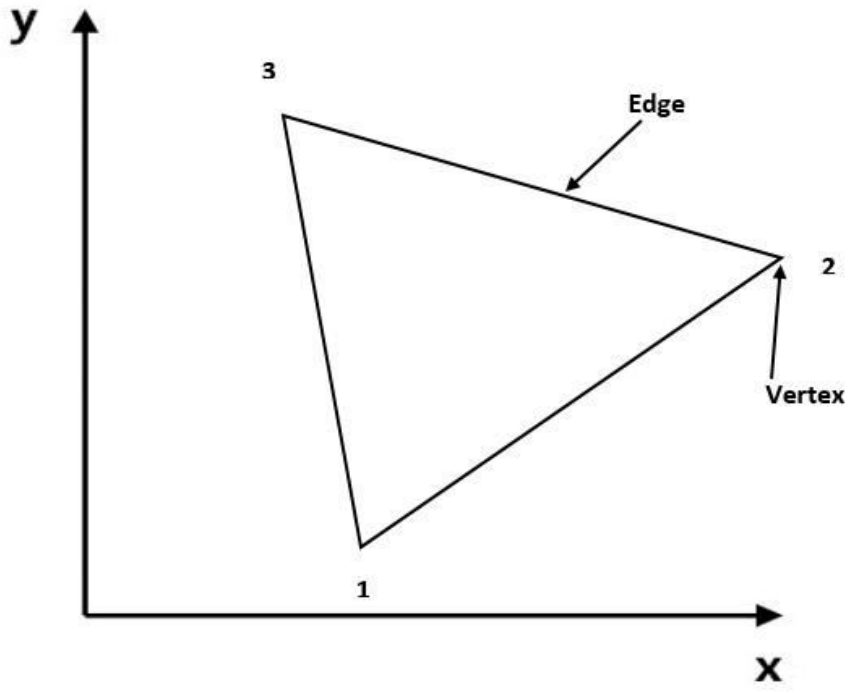

(a) Triangular Element

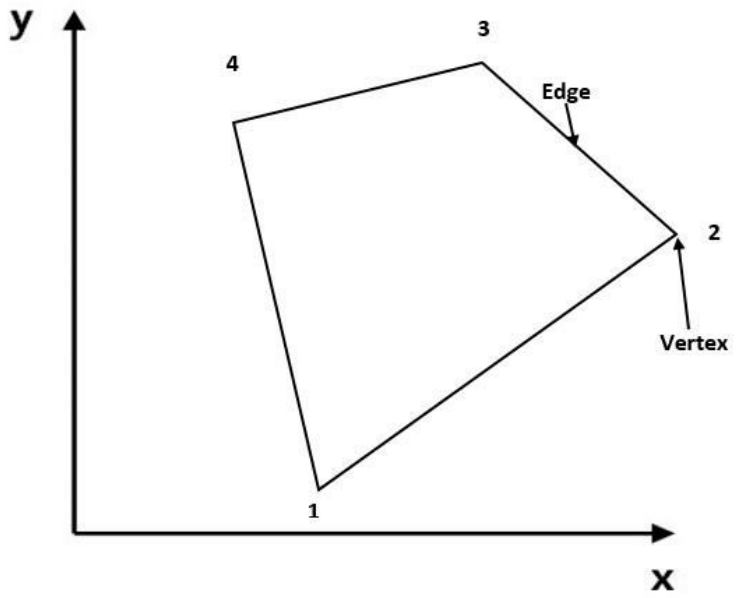

(b) Quadrangle Element

Fig. 4.7 Typical finite elements in the two dimensional x − y plane.

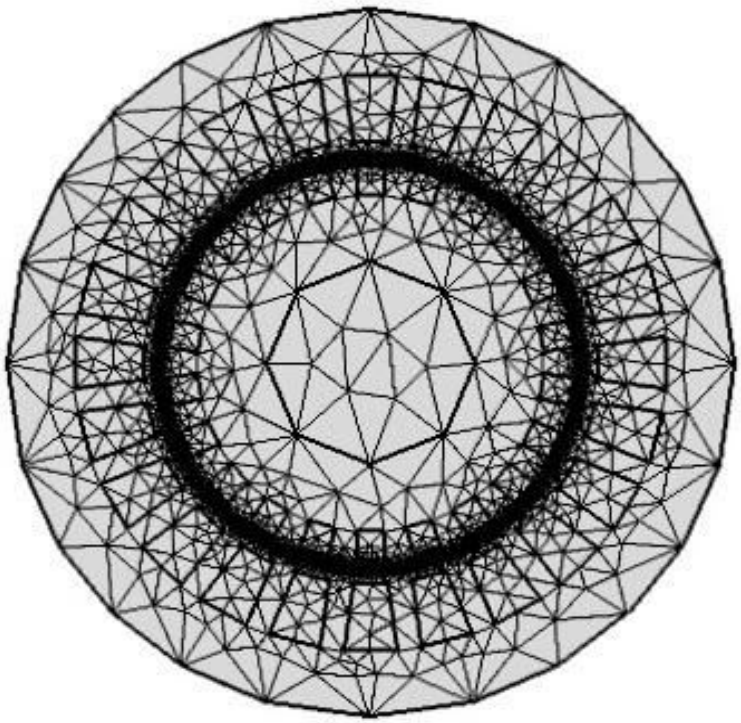

Fig. 4.8 Three phase induction motor is meshed by triangles

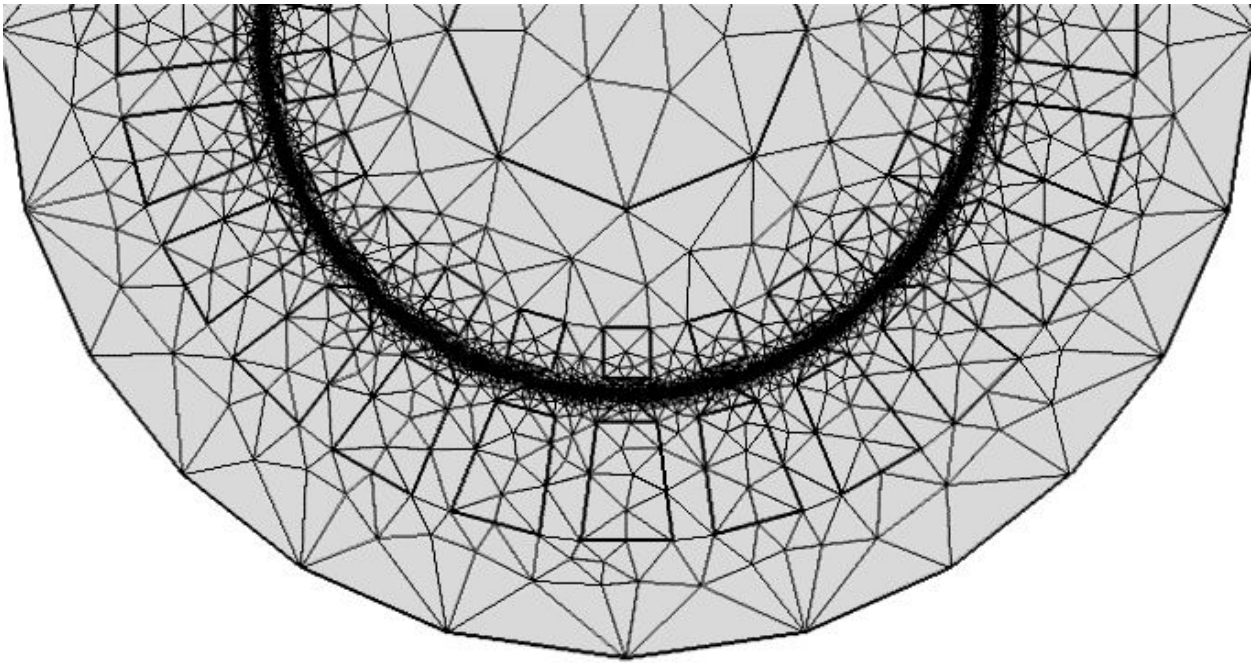

Fig 4.9 the enlarged region of the half of the three-phase motor

FEM mesh, as illustration, generated by COMSOL Multiphysics can be seen in Fig. 4.8. The arrangement of three-phase squirrel cage induction motor has been discretized by a triangular mesh as it is shown at the Fig. 4.8. In Fig 4.9, the enlarged region of the half of the three-phase motor is shown.

All the simulations have been studied using the same mesh, which consists of number of vertex elements: 392, number of boundary elements: 6496, number of elements: 21372, minimum element quality: 0.1465 and number of degrees of freedom solved for: 12330 as it can be seen in Fig. 4.8.

Air Gap Optimization:

Optimization of air-gap performed using parametric sweep which is shown in Fig. 4.10.

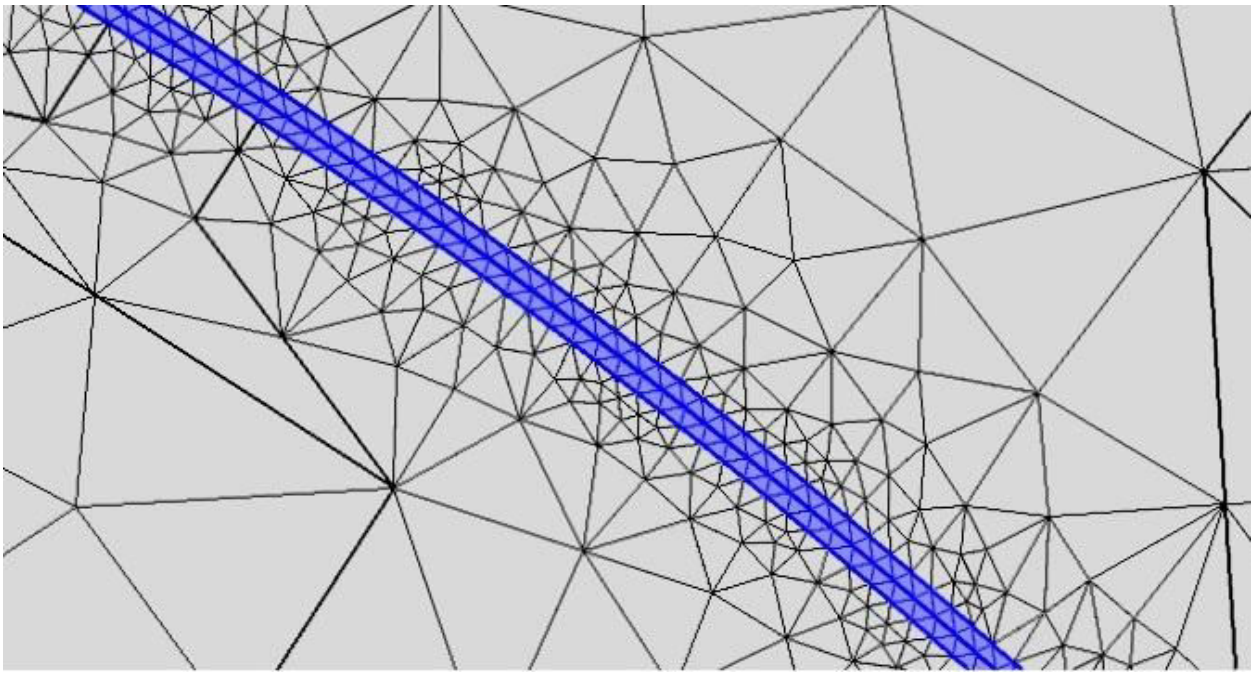

Fig. 4.10: Air gap meshing

Air-gap length is very important parameter which needs to be properly designed to get required torque and performance from the induction machine. It also helps engineers to design proper thickness of slot insulation since it indirectly influences the surface temperatures of the machine. Parametric sweep on air-gap has performed in a range of 0.00003m – 0.001m and found minimum element quality equal to 0.1465004mm as the optimal for better performance of the machine. Indeed, this parametric sweep has contributed for optimization of machine performance and torque by considering correct thickness of air-gap. Results obtained are close to the standard induction motor characteristics. This can also be used to optimize various performance characteristics of the machine.

5. Chapter V

Result and Discussion

5.1 introduction:

Problem designed induction motor is modeled in COMSOL Multiphysics for simulation. First of all, this healthy model has been verified with some characteristics of IM. After successfully verified, we have model for other condition like faulted condition, broken condition etc. Therefore, inter turn fault condition is modeled and analysed the results with healthy condition. The total number of turns of the IM is 1248 (each phase 416 turns). Inter turn fault is modeled by reducing the number turn of one phase. Inter turn fault is considered in one phase only. We have taken six sample

1. Healthy condition.
2. Faulty condition with 2 turn short (0.48%fault of phase1)
3. Faulty condition with 4 turn short (0.96%fault of phase1)
4. Faulty condition with 6 turn short (1.44%fault of phase1)
5. Faulty condition with 8 turn short (1.92%fault of phase1)
6. Faulted condition with 116 turn short (27.8%fault of phase1)

5.2 Validation of Model:

The validation of the model is done with no load. The supply voltage is 400 Volt (V_{rms}=400 Volt; $V_{peak} = 400\sqrt{2}$ Volt) which is shown in Fig. 5.1. The validation characteristics are torque, no load current and speed of the motor. The values are compared in table 5.1 and the diagrams are given in Fig. 5.2, Fig 5.3, and Fig. 5.4 respectively. Corresponding Geometry with one phase coils, flux density norms, current density norms are shown in Fig. 5.5, Fig. 5.6 and Fig.5.7 Respectively.

SL. No.	Parameters	Theoretical value	Simulation value
1	Maximum Torque	29.58 (in N-m)	30.4 (in N-m)
2	No load current(Peak current)	1.414 (in A)	1.46 (in A)
3	No lad speed	≈ 157.08(in rad/s)	=156.64 (in rad/s)

Table 5.1: Validation of parameters

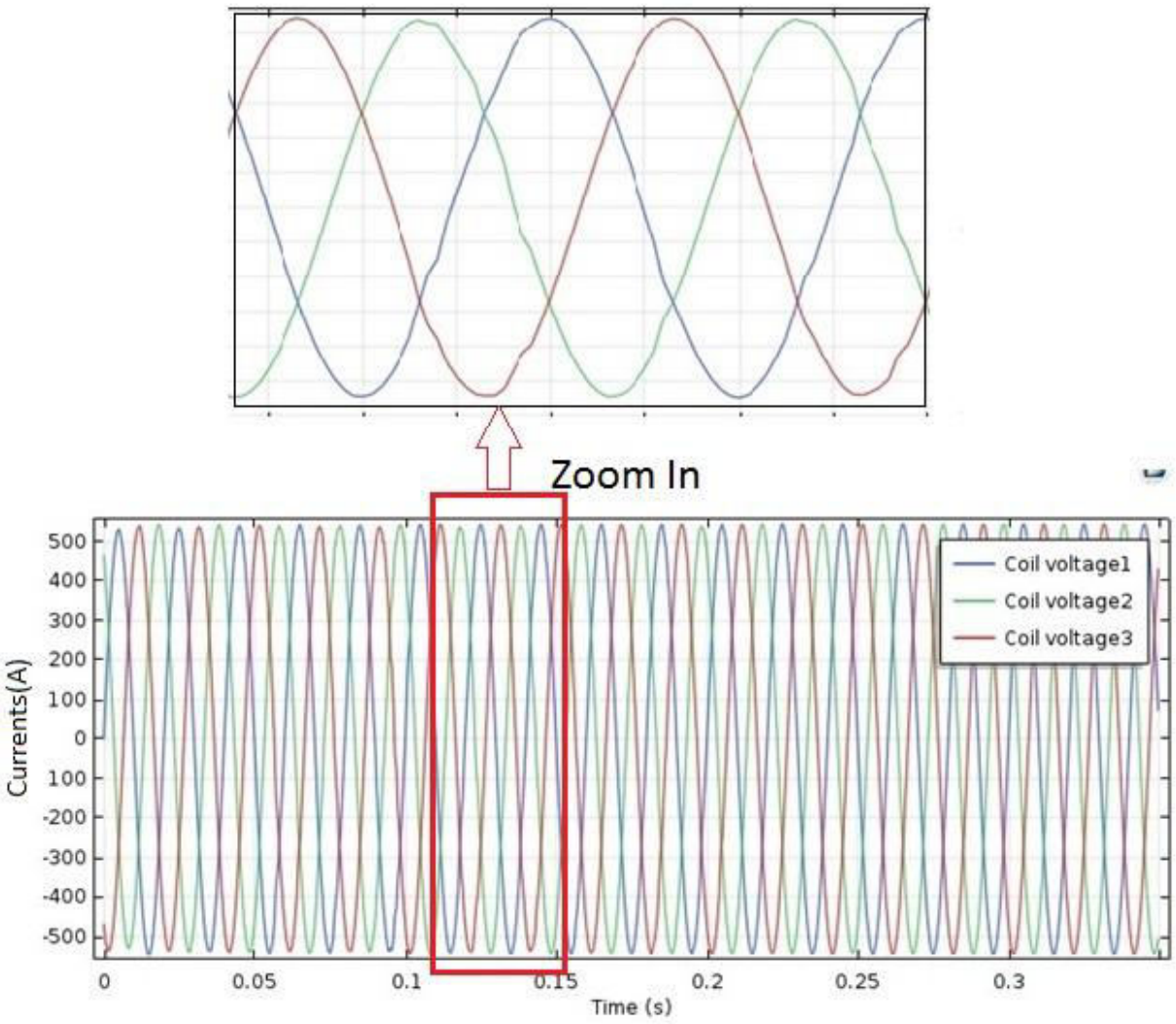

Fig.5.1: Three phaseCoil Voltage of stator

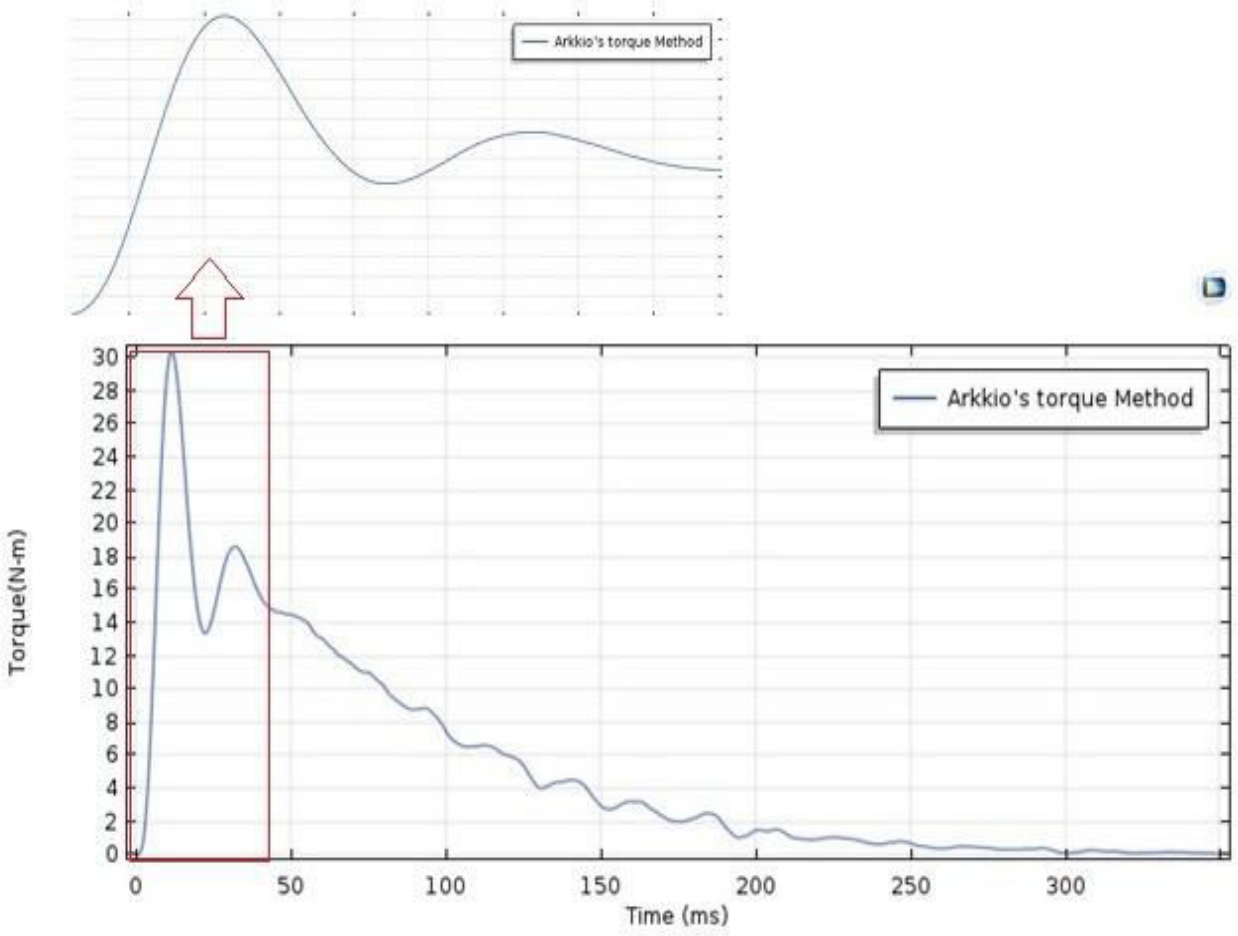

Fig.5.2: Torque vs time characteristics

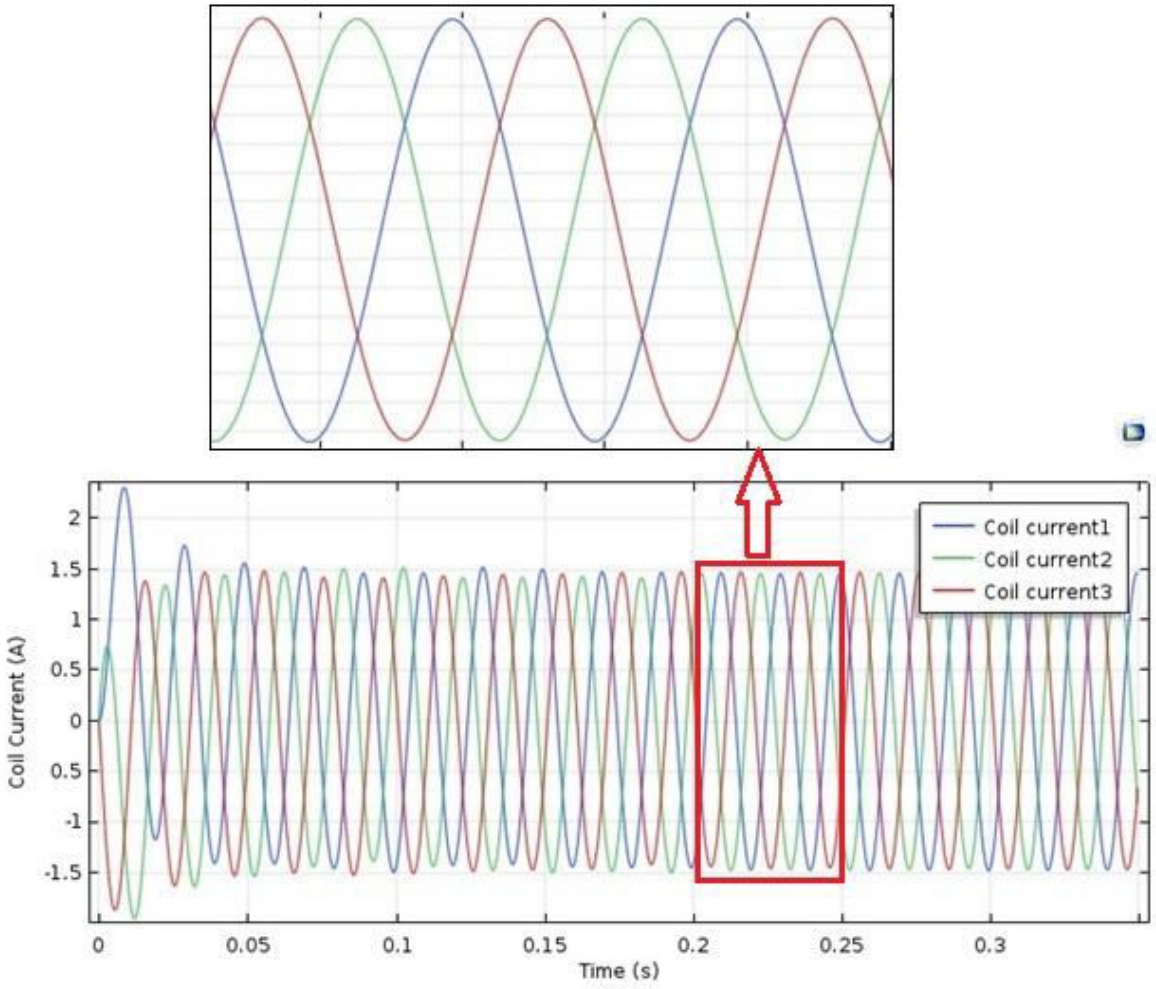

Fig. 5.3: No load 3 phase current of stator

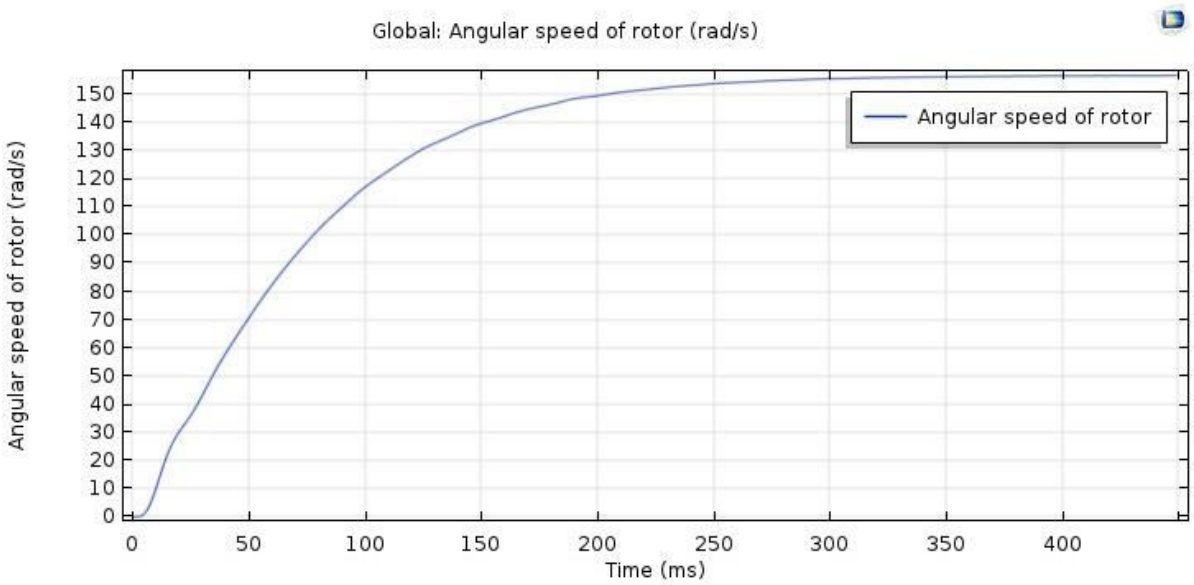

Fig. 5.4: No load speed vs time characteristic

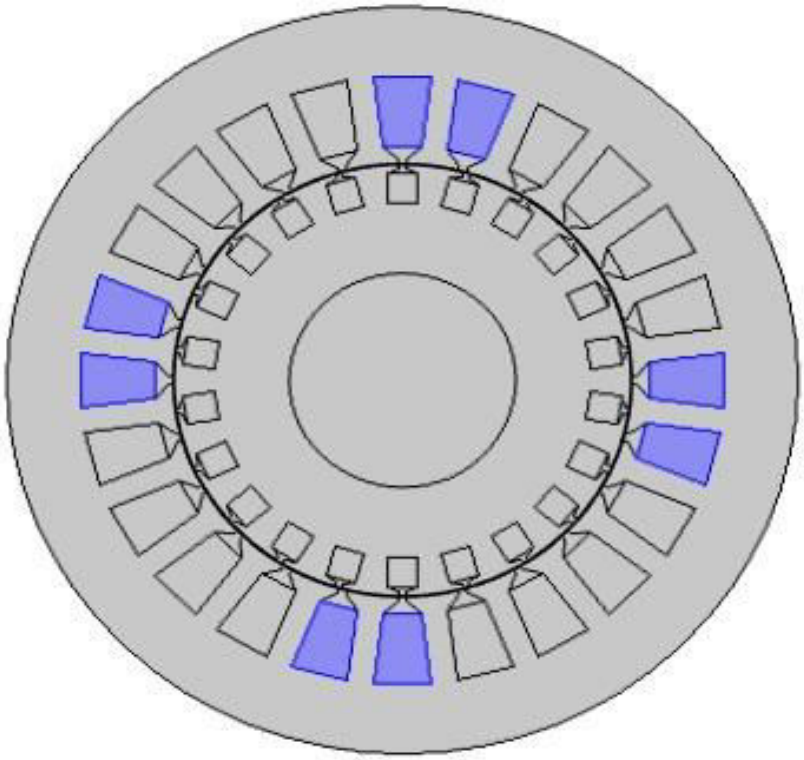

Fig. 5.5: Motor 2D model with one phase coils

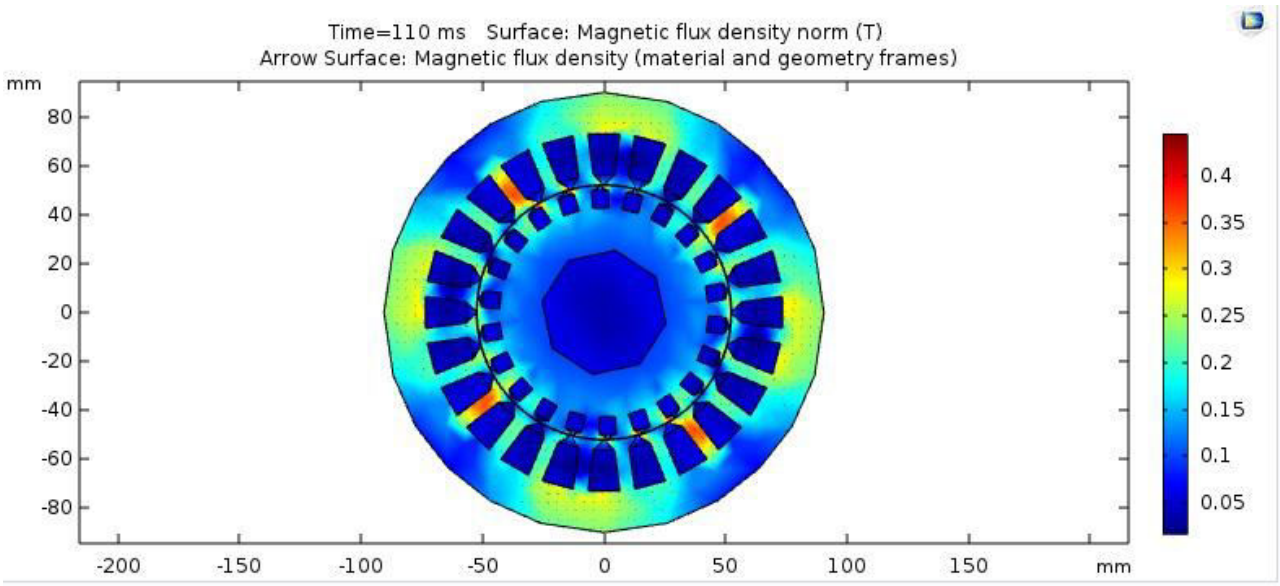

Fig. 5.6: Magnetic Flux density norm

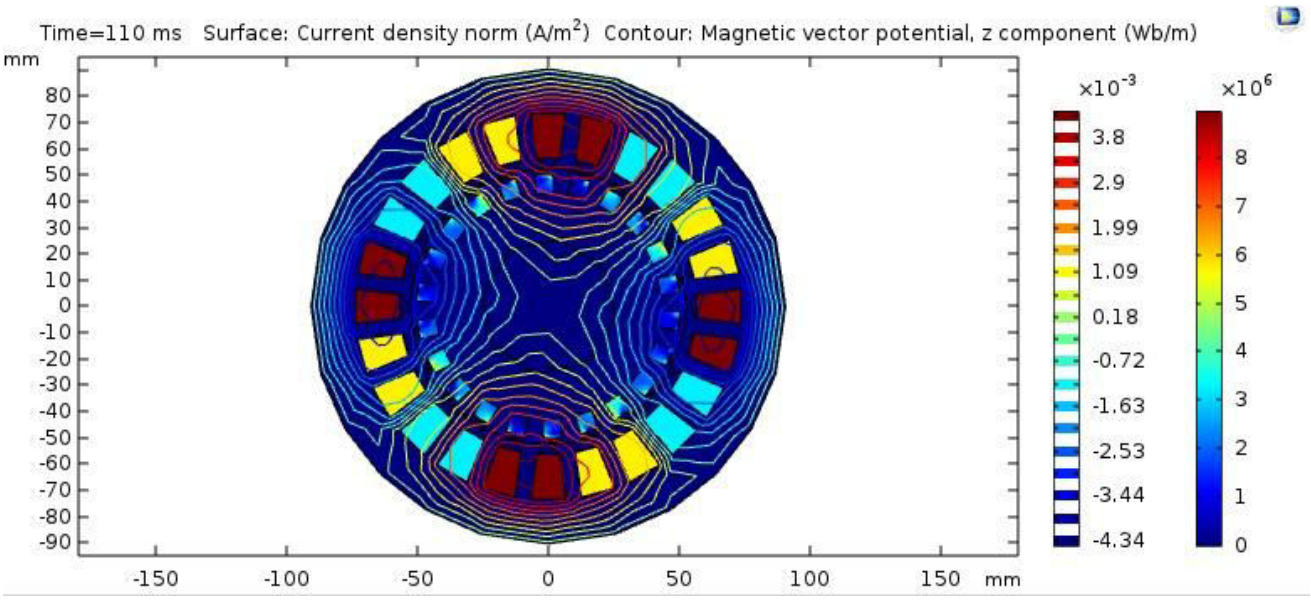

Fig.5.7: Current Density Norm

5.3 Results of Healthy and Faulty condition:

We have modeled with six sample which is mentioned in starting of this chapter. These are modeled as full load with speed of 1416 rpm (Full load slip 5.3%). The results (Stator coil voltage, stator coil current) of these sample are shown below individually.

1. **Healthy Condition**: The results of stator coil voltages and stator coil currents in this condition are shown in Fig. 5.8 and Fig. 5.9 respectively.

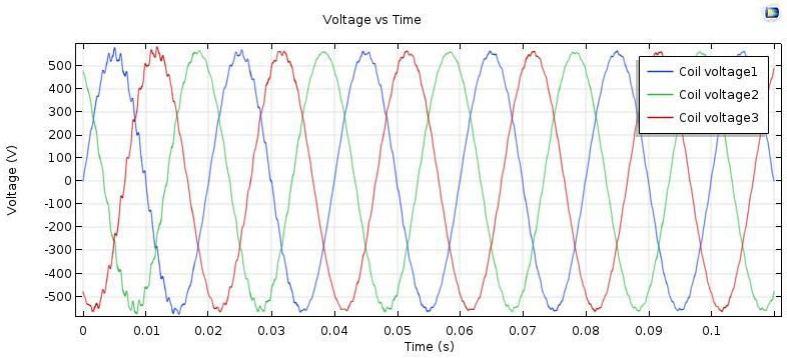

Fig. 5.8: Stator coil voltage for healthy condition

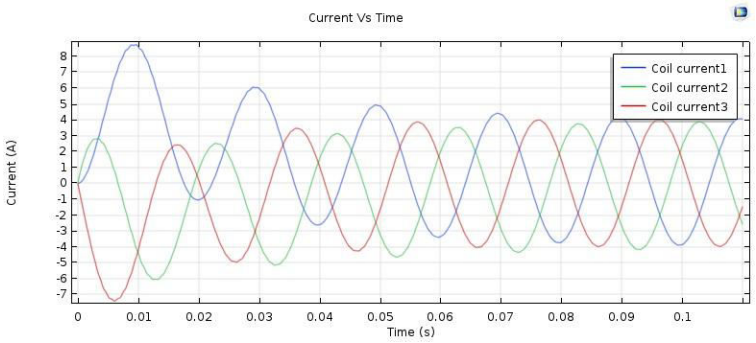

Fig 5.9 Stator coil current for healthy condition

2. **Faulty condition considering 2 turns short:** The results of stator coil voltages and stator coil currents in this condition are shown in Fig. 5.10 and Fig. 5.11 respectively.

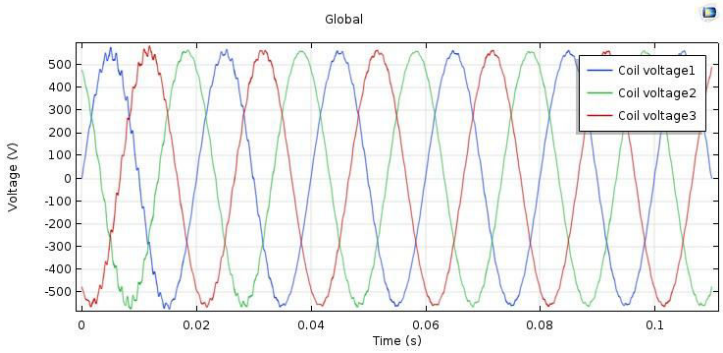

Fig. 5.10: Stator coil voltages for faulty condition considering 2 turns short.

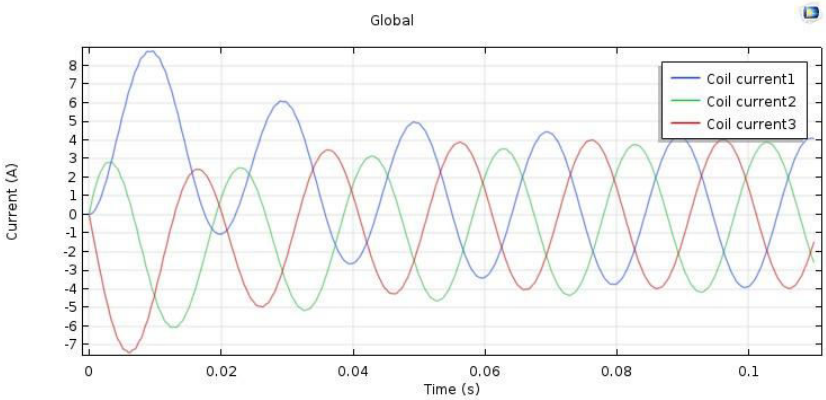

Fig. 5.11: Stator coil current for faulty condition considering 2 turns short.

3. **Faulty condition considering 4 turns short:** The results of stator coil voltages and stator coil currents in this condition are shown in Fig. 5.12 and Fig. 5.13 respectively.

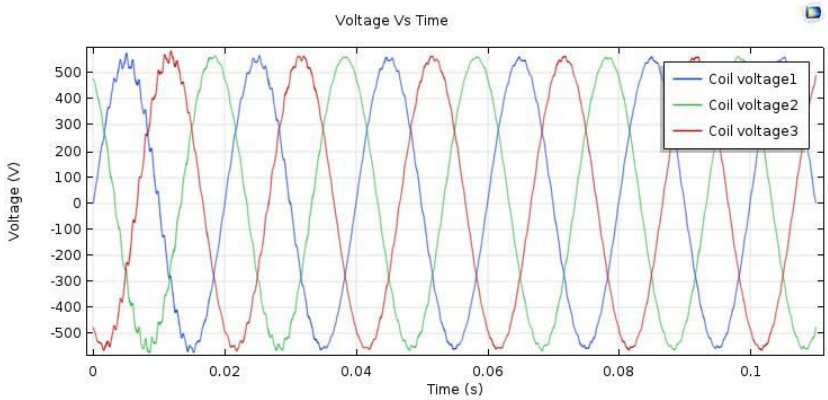

Fig. 5.12: Stator coil voltage for faulty condition considering 4 turns short.

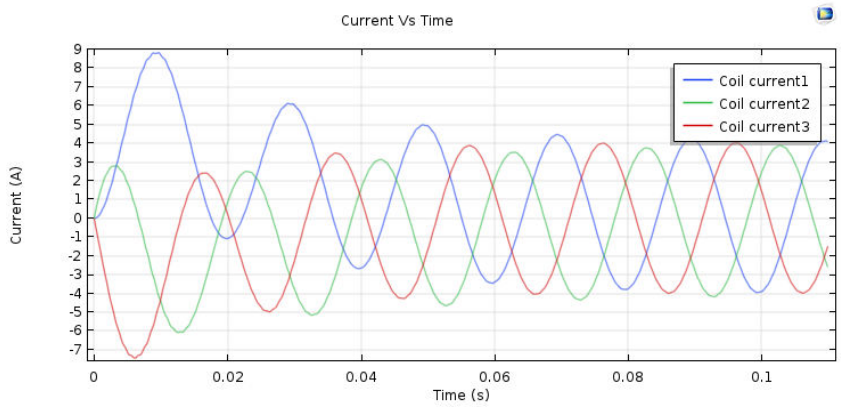

Fig. 5.13: Stator coil current for faulty condition considering 4 turns short.

4. **Faulty condition considering 6 turns short:** The results of stator coil voltages and stator coil currents in this condition are shown in Fig. 5.14 and Fig. 5.15 respectively.

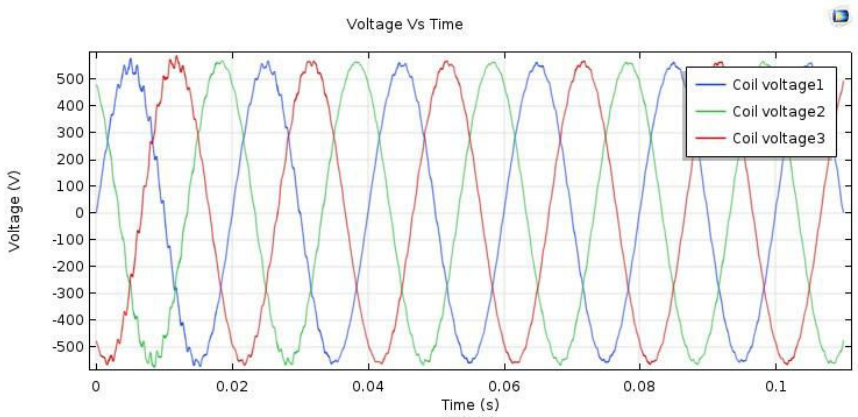

Fig. 5.14: Stator coil voltage for faulty condition considering 6 turns short.

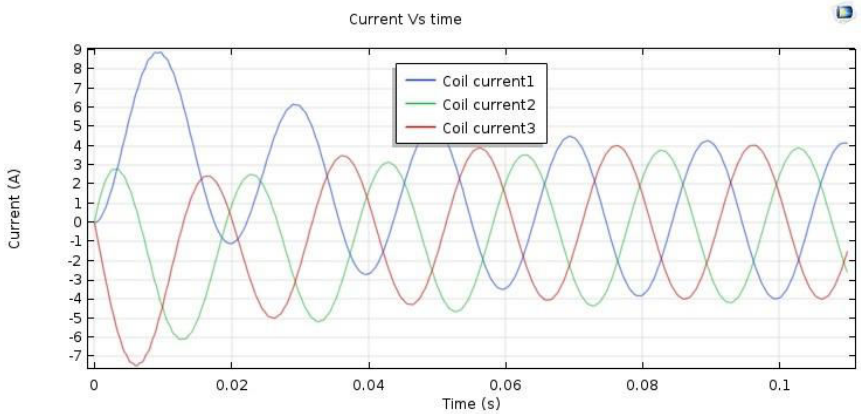

Fig. 5.15: Stator coil current for faulty condition considering 6 turns short.

5. **Faulty condition considering 8 turns short:** The results of stator coil voltages and stator coil currents in this condition are shown in Fig. 5.16 and Fig. 5.17 respectively.

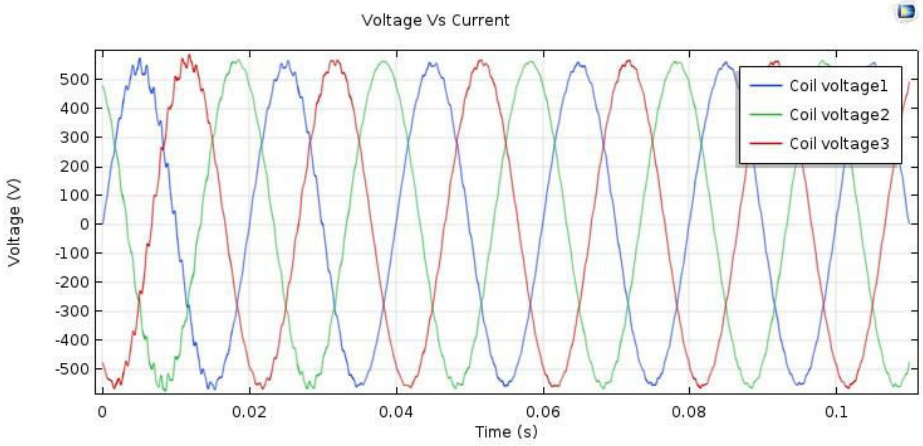

Fig. 5.16: Stator coil voltage for faulty condition considering 8 turns short.

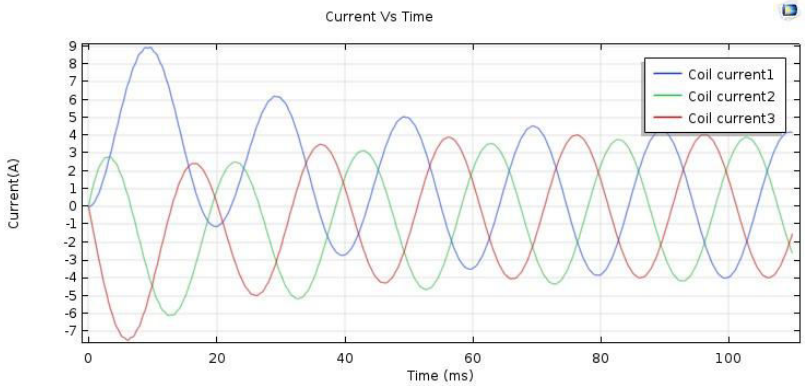

Fig. 5.17: Stator coil current for faulty condition considering 8 turns short.

6. **Faulty condition considering 116 turns short:** The results of stator coil voltages and stator coil currents in this condition are shown in Fig. 5.18 and Fig. 5.19 respectively.

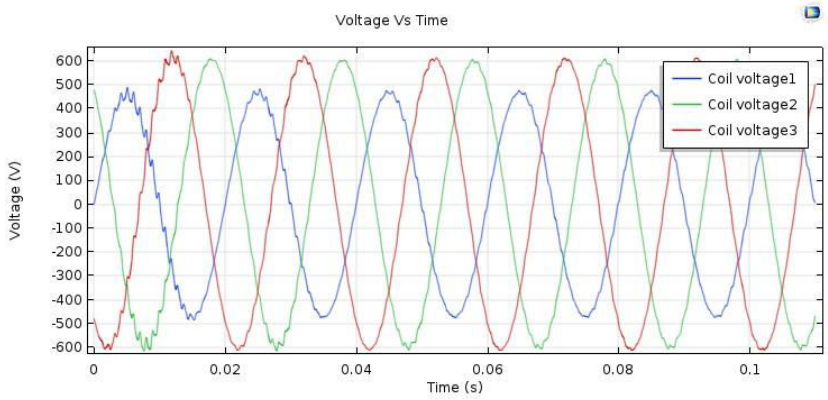

4.18: Stator coil voltage for faulty condition considering 116 turns short.

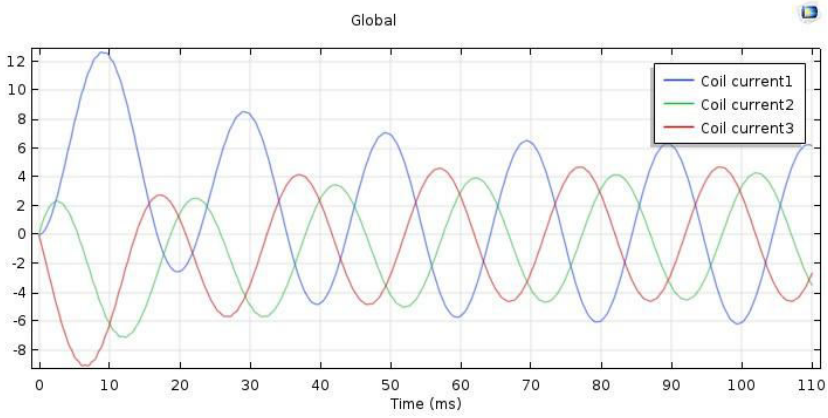

Fig. 5.19: Stator coil current for faulty condition considering 116 turns short.

5.4 Method of Stator Current Analysis:

If we supply sinusoidal power into the 3-Ø induction motor there will be harmonics because of slots in stator and slots in rotor. [8-10, 17-24] These harmonics magnitude could be changed or harmonics itself could be changed due to various fault in the induction motor. So we can analyse the harmonics characteristics for various faulted conditions. Some of faults have been noted below which is more severe for induction motor.

1. Short circuit fault
2. Rotor bar fault
3. Rotor ring fault

4. Bearing fault
5. Air-gap eccentricity

In this thesis we only analyse the characteristics of current for Inter-turn fault which is belong to short circuit fault.

If we take the consideration of stator and rotor slot, the good approximation of permeance of the air gap is [16]

$$\lambda(\theta,t) = \frac{\lambda_s(\theta,t)\lambda_R(\theta,t)}{\delta(\theta,t)} \quad 5.1$$

Where $\delta(\theta,t)$ is the radial air gap length, which can be taken as constant ($\delta(\theta,t) = \delta_0$) (assuming air-gap is equal in all radial aspects).

$\lambda_s(\theta,t)$ is the permeance of the air-gap without effect of the rotor slot,

$$\lambda_s(\theta,t) = \frac{1}{K_{C_S}} + \sum_{n_s=1}^{\infty} \lambda_{n_s} \cos(n_s S\theta) \quad 5.2$$

Where K_{C_S} is the Carter factor, λ_{n_s} is the amplitude of permeance related to the stator, n_s is the any integer, S is the number of total stator slot, θ is the angular position referring to stator.

$\lambda_R(\theta,t)$ is the permeance of the air gap without effect of stator slots.

$$\lambda_R(\theta,t) = \frac{1}{K_{C_R}} + \sum_{n_r=1}^{\infty} \lambda_{n_r} \cos(n_r R\theta - n_r R w_r t) \quad 5.3$$

Where K_{C_R} is the Cater factor, λ_{n_r} is the amplitude of permeance related to the rotor, n_r is the any integer, R is the number of total rotor slots or bar,

w_r is the rotor rotating angular frequency (Mechanical rotational speed),

$$w_r = w_s(1-s) = \frac{(1-s)}{p} w \quad 5.4$$

Where w_s is the synchronous rotating speed of the fundamental MMF, s is the sleep, p is the pole pair, *w* is the fundamental angular frequency of supply.

If we neglect the Carter facto part of the equation (5.2) and (5.3) we get,

$$\lambda_s(\theta,t) = \sum_{n_s=1}^{\infty} \lambda_{n_s} \cos(n_s S\theta) \quad 5.5$$

And

$$\lambda_R(\theta,t) = \sum_{n_r=1}^{\infty} \lambda_{n_r} \cos(n_r R\theta - n_r R w_r t) \quad 5.6$$

By putting the value of$\lambda_s(\theta,t)$, $\lambda_R(\theta,t)$ and ($\delta(\theta,t)$ in the equation (5.1) we get,

$\delta(\theta,t) = \sum_{n_r=1}^{\infty} \sum_{n_s=1}^{\infty} \lambda_{n_s}\lambda_{n_r} \cos(n_s S\theta) \cos(n_r R\theta - n_r R w_r t)$

$$\delta(\theta,t)=\sum_{n_r=1}^{\infty}\sum_{n_s=1}^{\infty}\frac{\lambda_{n_s}\lambda_{n_r}}{2}[\cos(n_sS\theta+n_rR\theta-n_rRw_rt)+\cos(n_sS\theta-n_rR\theta+n_rRw_rt)] \quad 5.7$$

Now, stator MMF without effect of skew can be represented by [16]

$$F_M(\theta,t)=\sum_{n_{\theta f}=1}^{\infty}\sum_{n_{wf}=-\infty}^{\infty}F_{n_{\theta f},n_{wf}}\cos(n_{\theta f}p\theta-n_{wf}wt) \quad 5.8$$

Flux density can be write as

$B(\theta,t)=F_M(\theta,t)\lambda(\theta,t)$

$=\sum_{n_r=1}^{\infty}\sum_{n_s=1}^{\infty}\sum_{n_{\theta f}=1}^{\infty}\sum_{n_{wf}=-\infty}^{\infty}B_{nr,ns,\theta f,wf}\cos(n_{\theta f}p\theta-n_{wf}wt)\{\cos(n_sS\theta+n_rR\theta-n_rRw_rt)+\cos(n_sS\theta-n_rR\theta+n_rRw_rt)\}$

$$B(\theta,t)=\sum_{m_{1,\Omega}}^{\infty}B_{m_{1,\Omega}}\cos(m_1\theta-\Omega t)+\sum_{m_{2,\Omega}}^{\infty}B_{m_{2,\Omega}}\cos(m_2\theta-\Omega t) \quad 5.9$$

Where

$$m_1=n_{\theta f}p\pm(n_sS+n_rR)$$

$$m_2=n_{\theta f}p\pm(n_sS-n_rR)$$

$$\Omega=n_rRw_r\pm n_{wf}w$$

Then, the change in the flux density distribution results in the current having harmonics as follows

$$f_{harmonics}=n_rRN_r\pm n_{wf}f \quad 5.10$$

Where $N_r=\frac{(1-s)}{p}f$ is the rotational speed of the rotor.

We can re-write the Eq. (5.10) as below

$f_{harmonics}=n_rR\frac{(1-s)}{p}f\pm n_{wf}f$

If we consider harmonic less MMF of stator then, $n_{wf}=1$ [3],

Therefore

$$\boldsymbol{f_{harmonics}=(n_rR\frac{(1-s)}{p}\pm 1)f} \quad 5.11$$

As per our model of IM, if we put the value of characters of equation (5.11), we get

$\boldsymbol{f_{harmonics}}$ **= 470.85, 570.85, 991.7, 1091.7, 1512.55, 1612.55 and so on**.

Where R= 22, s= 5.3%, p=2, f=50Hz and n_r= 1, 2, 3, 4, up to infinite.

5.5 Observations:

1. The current of faulted phase is increasing significantly if fault is ≈ 28% of particular phase which is shown in Fig. 5.20. As the current is increasing proportionally, the current will be more high if faulted portion will be increased.

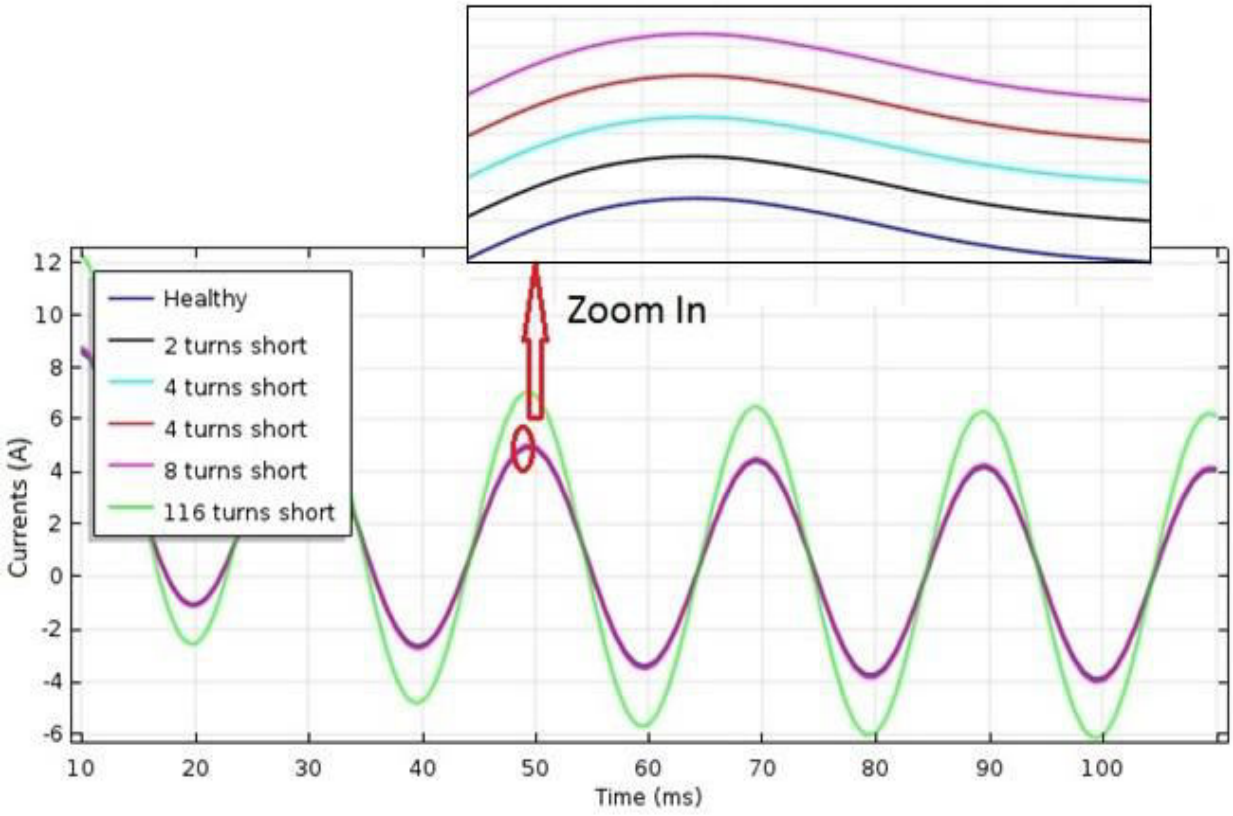

Fig. 5.20: Overlapping of healthy and faulty phase currents

2. Although 2nd phase's current and 3rd phase's currents value (which is 120 degrees and 240 degrees electrically apart from faulted phase) are increasing but no so great. These are shown in Fig. 5.21 and Fig. 5.22.

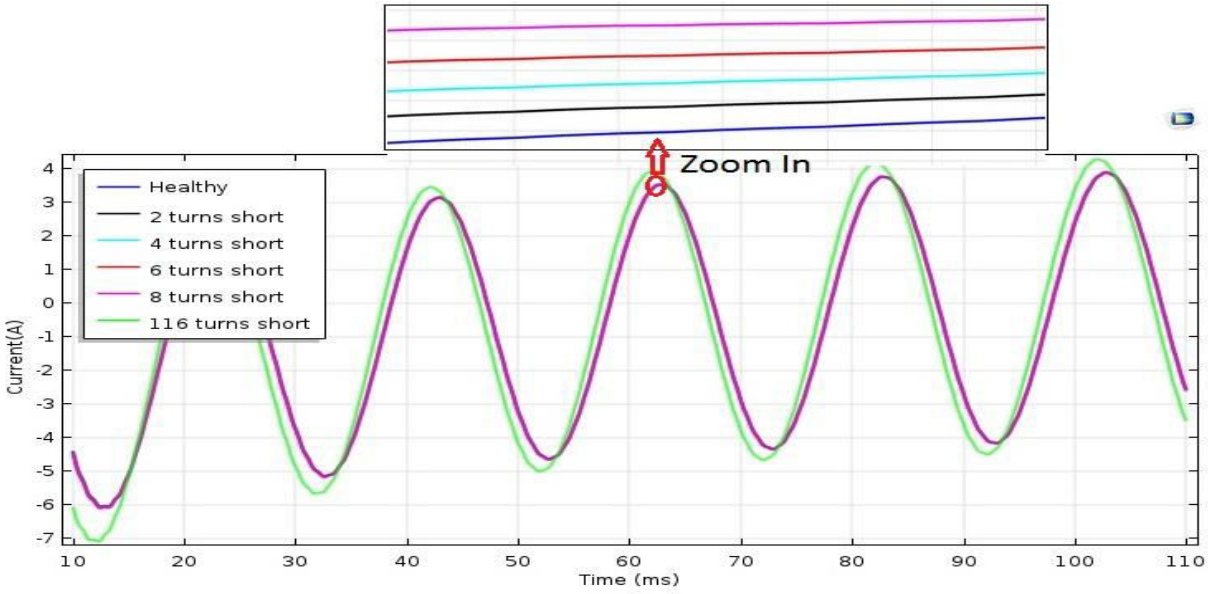

Fig. 5.21: 2nd phase's current waveform

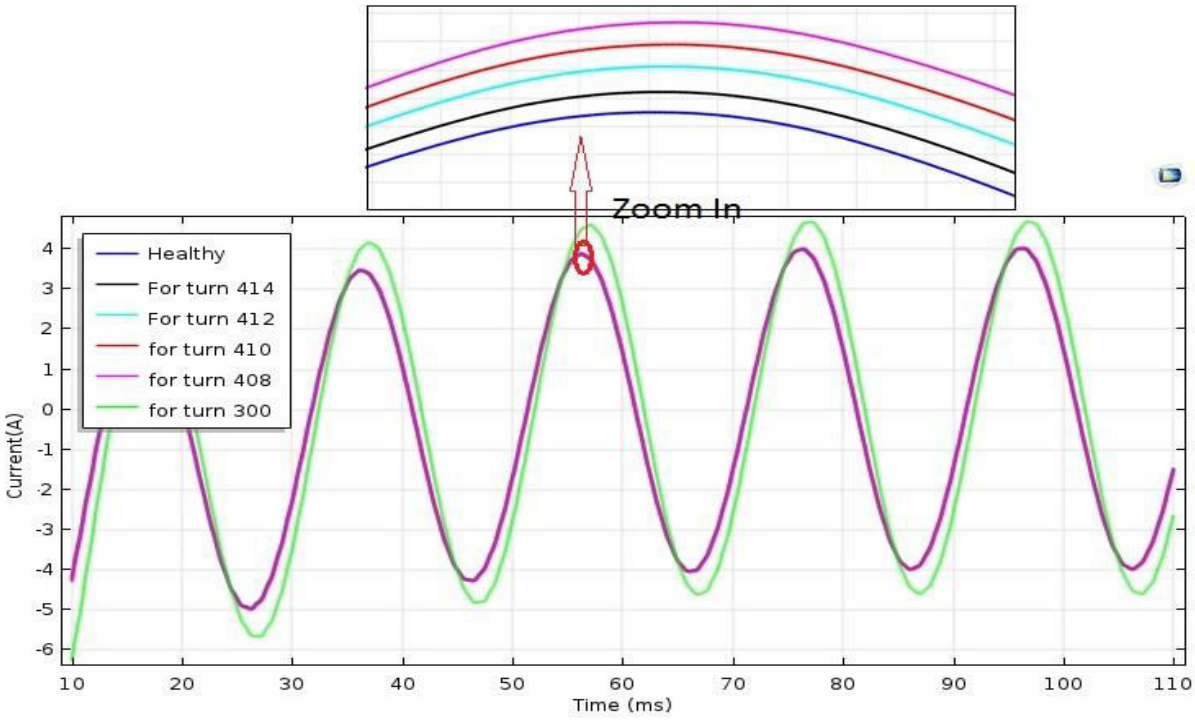

Fig. 5.22: 3rd phase's current waveform

3. For 2nd phase, current waveform is shifting left. For 3rd phase, current waveform is shifting right which are shown in Fig.23. This means zero crossing also shifting consequently.

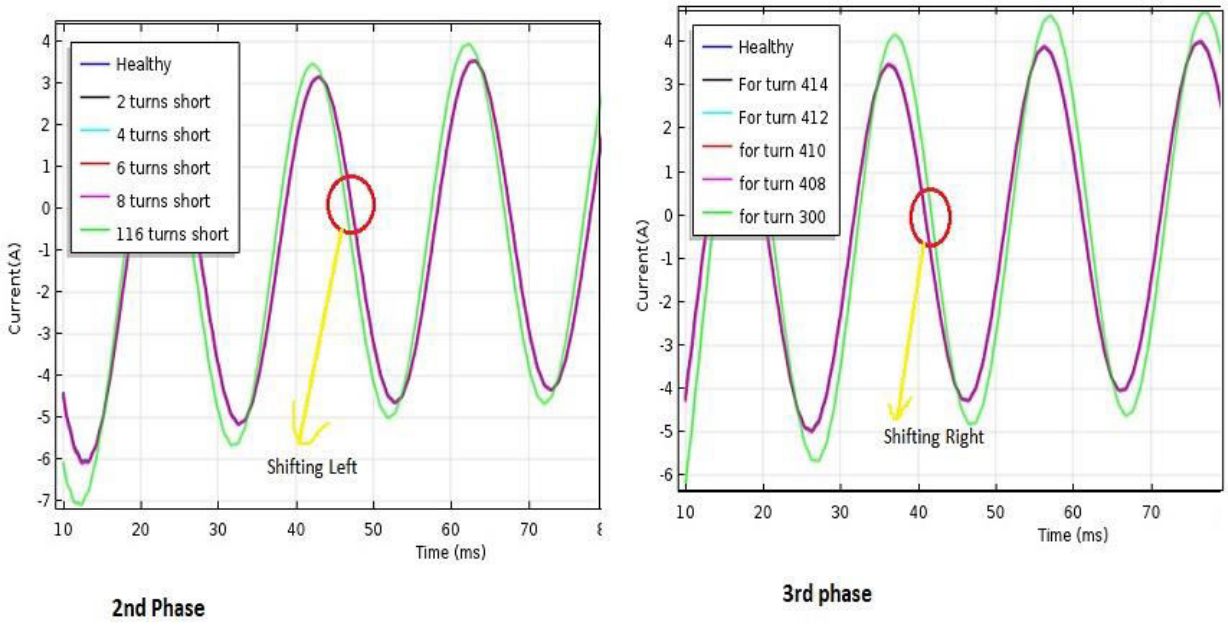

Fig. 23: current waveform of 2nd & 3rd phase considering phase shifting

4. Faulted phase current is plotted in frequency spectrum (Continuous FFT) and overlapped for all conditions which is shown in Fig.5.24.

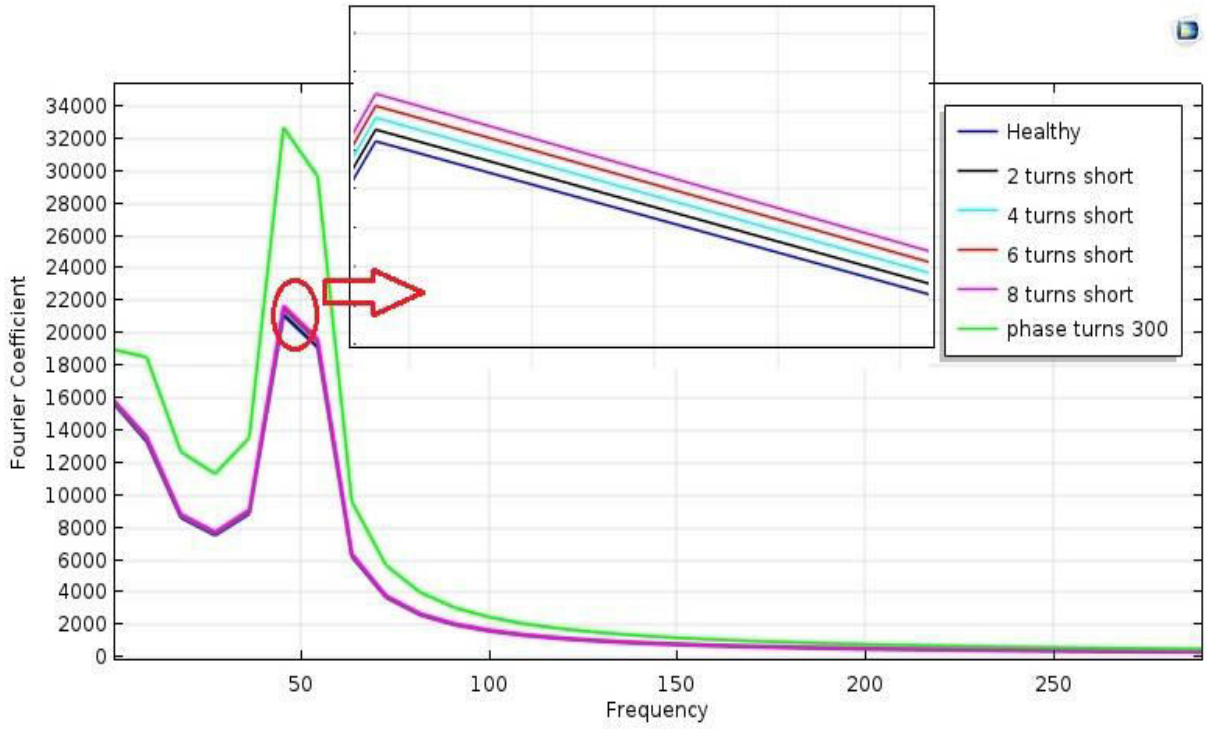

Fig.5.24: frequency spectrum (Continuous FFT) of faulted phase currents

5. The current density distribution is also changing significantly. The surface plot of the current distribution with healthy and faulty condition is shown in Fig. 5.24. Some change spots are highlighted. If you notice carefully, it's clear that the all stator slot current density for faulty phase(phase1), is decreasing and increasing for faulty phase (phase 1) and healthy phase (Phase2 and phase3) respectively.

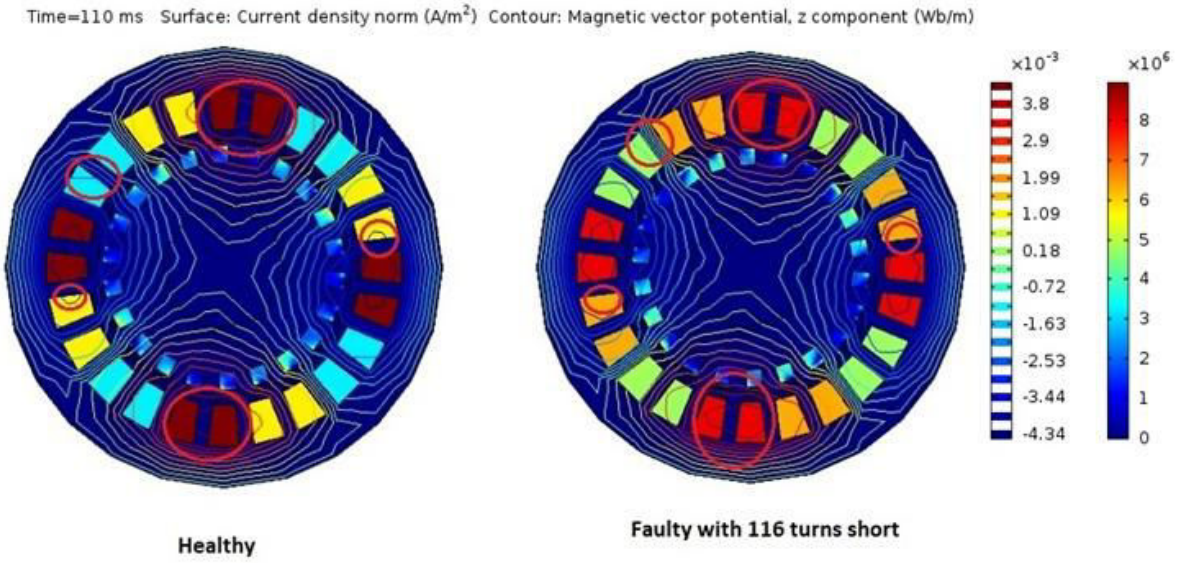

Fig. 5.25: Comparison of Current density between healthy and 116 short turn condition.

6. Chapter VI

Conclusion and Future Work

6.1 Conclusions:

In this thesis a 2-D FE modeling of a Squirrel Cage Induction Motor is presented. Then inter turn short circuit fault in the stator winding has been emulated. The modeling as well as the simulations carried out in COMSOL Multiphysics platform. After simulation the stator phase currents have been analysed. The FFT of the current shows that the slot harmonics are amplified with severity of the faults. That mean for experimental studies the slot harmonics are only to be considered for fault characterisation which will make the fault identification process much easy.

The IM which is chosen from IM design problem is not practiced one. FEM computation is more time consuming and needs super computer with sufficient RAM, good graphics memory and good computation speed. These considerations have been fulfilled as good as possible. But more compromised with less elements and less sampling points which may leads to more deviation from accurate one.

6.2 Scope of Future Work:

As mentioned in chapter of introduction that there is no such reliable method of detection of induction motor fault. And it is necessary to implement the reliable method of detection. The step has been taken with analysation of the inter-turn fault by FE modeling. Later this result can be used to implement the method of fault detection. Same way analysation of the other faults can be performed as well with the help of FE modeling. i.e.

1. Coil to coil fault
2. Phase to phase
3. Phase to ground
4. Broken bar
5. Brocken ring
6. Bearing fault

7. Chapter VII

Reference

[1] Dr. P.S. Bimbra., "Electrical Machinery" Khanna Publishers, New Delhi, 2013.

[2] Austin H. Bonnett, George C. Soukup "Cause and Analysis of stator and rotor Failures in three phase Squirrrel Cage Induction Motots" IEEE Transactions ON Industry Applications, VOL. 28, NO. 4, JULY / AUGUST 1992.

[3] O. A. Mohammed, N. Y. Abed, and S. Ganu., "Modeling and Characterization of Induction Motor Internal Faults Using Finite-Element and Discrete Wavelet Transforms" IEEE Transactions ON Magnetics, VOL. 42, NO. 10, October 2006.

[4] www.Comsole.com

[5] A.K. Sawhaney, DR. A. Chakrabarti., "Electrical Machine Design" Dhanpat Rai & Co. (P) ltd, Nai Sarak, Delhi 2013

[6] Mohamed El Hachemi Benbouzid, "A Review of Induction Motors Signature Analysis as a Medium for Faults Detection" IEEE Transactions ON Industrial Electronics, VOL. 47, NO. 5, October 2000.

[7] Zhongming Ye, Bin Wu and Alireza Sadeghian., "Current Signature Analysis of Induction Motor Mechanical Faults by Wavelet Packet Decomposition" IEEE Transactions on Industrial Electronics, VOL. 50, NO. 6, December 2003.

[8] M. Farzam Far, A. Arkkio and J., "Electrical Fault Diagnosis for an Induction Motor Using an Electromechanical FE Model" IEEE Transaction

[9] Matthew N. O. Sadiku "Principle of Electromagnetics" Oxford University Press, New Delhi, 2009.

[10] http://mathworld.wolfram.com/

[11] P.K. Banerjee., "The Boundary Method of Engineering" McGRAW-HILL Book Compreney Europe, England

[12] Jacek F. Gieras, Mitchell Wing. "Permanent Magnet Motor Technology Design and Application" Marcel Dekker Inc., New York, Basel, 2002.

[13] N. Sadowski(*), Y. Lefevre, M. Lajoie-Mazenc, J. Cros "finite element torque calculation in electrical machines while considering the movement" IEEE Transactions on Magnetics, VOL. 28, N0.2, March 1992

[14] https://www.hindawi.com/journals/mpe/2017/2640796/

[15] M. Blödt, P. Granjon, B. Raison, and G. Rostaing, "Models for bearing damage detection in induction motors using stator current monitoring," IEEE Transactions on Industrial Electronics, vol. 55, no. 4, 2008

[16] P. Frauman, A. Burakov, and A. Arkkio, “Effects of the slot harmonics on the unbalanced magnetic pull in an induction motor with an eccentric rotor,” IEEE Transactions on Magnetics, vol. 43, no. 8, 2007

[17] A. H. Bonnet, “Analysis of winding failures in three-phase squirrel cage induction motors,” IEEE Trans. Industrial Applications, vol. 14, no. 3, 1978.

[18] G.C. Stone, B.K. Gupta, “Investigation of turn insulation failure mechanisms in large AC Motors,” IEEE Trans. Power Apparatus Systems, vol. 103, no. 9, 1984.

[19] J. Penman, H.G. Sadding, B.A. Lloyd, W.T. Fink, “Detection and location of interturn short Circuits in the stator windings of operating motors,” IEEE Trans. Energy Conversion, vol. 9, No. 4, 1994.

[20] G.M. Joksimovic, J. Penman, “The Detection of Inter-Turn Short Circuits in the Stator Windings of Operating Motors,” IEEE Trans. Industrial Electronics, vol. 47, no. 5, 2000.
[21] A. Stavrou, H.G. Sedding, J. Penman, “Current Monitoring for Detecting Inter-Turn Short Circuits in Induction Motors,” IEEE Trans. Energy Conversion, vol. 16, no. 1, 2001.
[22] W.T. Thomson, “On-line MCSA to diagnose shorted turns in low voltage stator windings Of three-phase induction motors prior to failure,” in proc. IEEE PES & IAS IEMDC, Boston, MA, 2001.
[23] C. Gerada et al, “The results do mesh,” IEEE Industry Applications Magazine, vol. 13, Issue 2, 2007.
[24] A. Bellini, F. Filippetti, C. Tassoni, G.A. Capolino, “Advances in diagnostic techniques for Induction machines,” IEEE Trans. Industrial Electronics, vol. 55, issue 12, 2008.
[25] P.J. Rodrigues, “Current, force, and vibration-based techniques for induction motor condition monitoring” Research gate, 2007.
[26] J. R. Stack, T. G. Habeter, and R. G. Harley, “Fault classification and fault signature production for rolling element bearings in electric machines,” IEEE Transactions on Industry Applications, 2004.
[27] M. Blödt, P. Granjon, B. Raison, and G. Rostaing, “Models for bearing damage detection in induction motors using stator current monitoring,” IEEE Transactions on Industrial Electronics, 2008.
[28] Mahdi Karami, Norman Mariun, Mohammad Rezazadeh Mehrjou, Mohd Zainal Abidin Ab Kadir, Norhisam Misron, and Mohd Amran Mohd Radzi,"Static Eccentricity Fault Recognition in Three-Phase Line Start Permanent Magnet Synchronous Motor Using Finite Element Method" Centre for Advanced Power and Energy Research, Faculty of Engineering, Universiti Putra Malaysia, 43400 Serdang, Selangor, Malaysia, 2014.